# Collective spontaneous emission from a line of atoms

J. P. Clemens,[1,2] L. Horvath,[1,3] B. C. Sanders,[3] and H. J. Carmichael[1,2,*]
[1]*Department of Physics, University of Oregon, Eugene, Oregon 97403-1274, USA*
[2]*Department of Physics, University of Auckland, Private Bag 92019, Auckland, New Zealand*
[3]*Department of Physics, Macquarie University, Sydney, New South Wales 2109, Australia*
(Received 21 February 2003; published 25 August 2003)

We study collective spontaneous emission from a linear array of $N$ two-state atoms using quantum trajectory theory and without an *a priori* single-mode assumption. Assuming a fully excited initial state, we calculate the angular distribution of the $k$th emitted photon, $k=1,\ldots,N$. We investigate the evolution of the distribution from a dipole radiation pattern for the first photon emission to a distribution characteristic of directional superradiance. The formalism is developed around an unravelling of the master equation in terms of source-mode quantum jumps. Exact calculations for 11 and fewer atoms do not show directional superradiance, but are characterized by delayed (subradiant) photon emissions directed along the axis of the linear array. A modified boson approximation is made to treat the many-atom case, where it is found that strong directional superradiance occurs for a few hundred atoms; the decay of subradiant excitations is preserved in the tail of the superradiant pulse.

DOI: 10.1103/PhysRevA.68.023809 PACS number(s): 42.50.Fx, 42.50.Lc

## I. INTRODUCTION

Collective spontaneous emission is a problem of fundamental interest in quantum optics. It has attracted a great deal of attention since the seminal work of Dicke [1], especially in connection with the phenomenon of super-radiance [2,3]. Despite the attention, certain aspects of the problem are still not well understood. Among these is the angular dependence of the emission from a spatially extended sample of atoms. In this paper we investigate this, and related features of collective spontaneous emission, by developing the quantum trajectory theory of spontaneous emission from a linear array of two-state atoms. Our model reverts to the Dicke model of super-radiance when the line is much shorter than the resonant wavelength $\lambda_0$, and to a line of independently emitting atoms when the atom spacing is large compared with $\lambda_0$. In both these limits the distribution of emitted photons follows the dipole radiation pattern. A more complicated pattern is expected away from these limits. The principal aim of the paper is to demonstrate how, in this intermediate regime, a directional superradiant pulse can grow spontaneously from quantum noise, recognizing that the first photon is necessarily emitted with the dipole distribution.

The model studied is of broad theoretical interest as the simplest example of an extended medium; it requires that we develop the full multimode theory of collective spontaneous emission, yet may be realized with numbers of atoms that are not prohibitively large. Considering the current interest in quantum information and quantum computation, it also presents a fascinating example of a quantum dynamical process set within the Hilbert space of $N \gg 1$ ''qubits'' [4]. The Hilbert space is enormous, even for $N=100$ atoms and thus, exact quantum trajectories are uncomputable. A major part of our paper is therefore devoted to the formulation of useful, physically motivated approximations. An interesting direction for future work is the exploration of the physics that calls for the enormous Hilbert space in the first place.

We quote from Dicke's original paper [1]: ''A classical system of simple harmonic oscillators distributed over a large region of space can be so phased relative to each other that coherent radiation is obtained in a particular direction. It might be expected also that the radiating gas under consideration would have energy levels such that spontaneous radiation occurs in one particular direction.'' Dicke continues to discuss the emission from such a phased initial state. Emission of this sort was also discussed later by others, notably Rehler and Eberly [5], who provide a semiclassical treatment of both the directional and temporal characteristics of the emission. Our concern is with the fully excited initial state of a collection of two-state atoms. For this, there is no initial phasing of the atomic dipoles to dictate the direction of the emission, which is to be determined from the geometry of the atomic sample and orientation of the dipoles. Previous work on the topic developed the idea that the emitted photons tend to form a ''ray'' [6]. Alternatively, it has been argued, on the basis of the sample geometry, that a single-mode treatment of the emission process is justified [7–10]; such a treatment is attractive, since it is formally equivalent to the Dicke model of $N$ atoms within a cubic wavelength [1] for which the equations can be solved in a number of ways [11–17]. Work along these lines envisages an extended medium made up of a macroscopic number of atoms. In a somewhat different vein, other authors have studied the case of two [6,18,19], four [19], and up to six [20] atoms, each claiming a little insight into the problem of directional emission in an extended medium.

The message from these previous works is unclear and confusing. There appears to be much that is valid in the ray idea of Ernst and Stehle [6], assuming we may interpret the ray as emission from some sort of collective mode of the medium. It is not clear, however, that only one ''ray'' should be dominant, at least through the initial stages of the emission. The first photon is certainly emitted in the dipole radia-

*Electronic address: h.carmichael@auckland.ac.nz

 

tion pattern, and is hardly the sole determinant of the direction of an eventual ray. With regard to the single-mode theories, Ressayre and Tallet [21,22] attempted a justification, but concluded that it is ''not obvious that such a model is valid.'' Work on a few atoms only adds to the confusion. For two atoms, Lehmberg [18] obtained results which he finds in contradiction with Dicke's photon-correlation argument for the enhancement of emission in certain directions. Duncan and Stehle [19], on the other hand, building upon the ''ray'' idea, claim ''an unambiguous tendency for the emitted photons to go in a common direction.'' The claim is based on numerical calculations for a line of four atoms. Blank *et al.*, considering six atoms, obtain results more in line with Lehmberg's comment. The claim of Duncan and Stehle is dubious, as their calculations exclude all but near-axial modes, a restriction demanded by the memory limitations of their computer; their justification for this disconcertingly presumes their conclusion: ''linear arrangements ... are expected to radiate primarily along their axis'' [19].

The present work clears up the confusion. It is based upon a quantum trajectory unravelling [23] of a previously derived master equation [24–27] for collective spontaneous emission from an arbitrary spatial distribution of two-state atoms. Carmichael and Kim [28] formulated an unravelling in which the jump operators are associated with the detection of a photon emitted in direction $\boldsymbol{k}$. Here, we formulate an unravelling in terms of jump operators that refer to source modes—collective modes of the atomic sample—whose emission patterns suggest an identification with the rays of Ernst and Stehle. Our source modes extend the analysis of Ressayre and Tallet [21,22] and will be reported on more fully in another publication [29]. We formulate the problem in the manner of Dicke [30], by calculating the angular distribution of the $k$th emitted photon and investigating its evolution with increasing $k$; we do not assume, however, as Dicke does, that the atoms are far apart. We concern ourselves in this paper with the development of directionality in the average over an ensemble of many superradiant pulses. Correlations and shot-to-shot fluctuations are also accessible in our approach, but will be studied elsewhere.

The organization of the paper is as follows. We summarize the physical model and quantum trajectory formalism in Sec. II. In Sec. III we treat the emission from a few atoms in a line without further approximation. Two- and three-atom cases are solved analytically, and up to 11 atoms through numerical simulation. We find that 11 atoms is too few to satisfy the joint requirement on density and line length to produce a directional superradiant pulse. In Sec. IV we make a formal connection between directed emission and the source modes used to unravel the master equation. We also outline the boson approximation that provides the basis of our treatment for many atoms. We apply and develop the approximation in Sec. V, to show how a directional superradiant pulse emerges from the competition between many superradiant source modes. We discuss some limitations and extensions of our treatment in Sec. VI and present conclusions in Sec. VII.

## II. QUANTUM TRAJECTORY FORMALISM FOR ANGULAR DISTRIBUTIONS

### A. Model

The physical system considered consists of $N$ identical two-state atoms located at positions $r_i$, $i=1,\ldots,N$. For the present we leave the locations of the atoms unspecified, other than to assume that the distances between them are less than or of the order of the resonance wavelength; the atoms then radiate collectively due to their interaction with the common electromagnetic field. We assume that the atomic dipole moments are all aligned in direction $\hat{d}$. The master equation describing the evolution of the atomic density operator in the electric-dipole, rotating-wave, and Born-Markov approximations has been previously derived [18,24–27]. In the interaction picture, it is given by

$$\dot{\rho}=-i\sum_{i\neq j=1}^{N}\Delta_{ij}[\hat{\sigma}_{i+}\hat{\sigma}_{j-},\rho]+\frac{1}{2}\sum_{i,j=1}^{N}\gamma_{ij}(2\hat{\sigma}_{j-}\rho\hat{\sigma}_{i+}-\hat{\sigma}_{i+}\hat{\sigma}_{j-}\rho-\rho\hat{\sigma}_{i+}\hat{\sigma}_{j-}), \tag{1}$$

with

$$\Delta_{ij}=\gamma\frac{3}{4}\left\{-[1-(\hat{d}\cdot\hat{r}_{ij})^2]\frac{\cos\xi_{ij}}{\xi_{ij}}+[1-3(\hat{d}\cdot\hat{r}_{ij})^2]\left(\frac{\sin\xi_{ij}}{\xi_{ij}^2}+\frac{\cos\xi_{ij}}{\xi_{ij}^3}\right)\right\} \tag{2}$$

and

$$\gamma_{ij}=\gamma\frac{3}{2}\left\{[1-(\hat{d}\cdot\hat{r}_{ij})^2]\frac{\sin\xi_{ij}}{\xi_{ij}}+[1-3(\hat{d}\cdot\hat{r}_{ij})^2]\left(\frac{\cos\xi_{ij}}{\xi_{ij}^2}-\frac{\sin\xi_{ij}}{\xi_{ij}^3}\right)\right\}, \tag{3}$$

where

$$\xi_{ij}\equiv k_0 r_{ij}=2\pi r_{ij}/\lambda_0, \quad \boldsymbol{r}_{ij}=r_{ij}\hat{r}_{ij}\equiv\boldsymbol{r}_i-\boldsymbol{r}_j; \tag{4}$$

$\gamma$ is the Einstein $A$ coefficient, $\lambda_0$ is the resonant wavelength, and atom $j$ has pseudospin operators $\hat{\sigma}_{j-}$, $\hat{\sigma}_{j+}$, and $\hat{\sigma}_{jz}$, which obey the commutation relations

$$[\hat{\sigma}_{i+},\hat{\sigma}_{j-}]=\delta_{ij}\hat{\sigma}_{iz} \quad [\hat{\sigma}_{i\pm},\hat{\sigma}_{jz}]=\mp 2\delta_{ij}\hat{\sigma}_{i\pm}. \tag{5}$$

The terms proportional to $\Delta_{ij}$ in the master equation account for dipole-dipole interactions and those proportional to $\gamma_{ij}$ account for the collective spontaneous emission. Due to the Markov approximation, the master equation does not account fully for propagation effects. For it to be valid, the sample

must not be too large; a photon must traverse it in a time much shorter than the characteristic time scale of the collective radiative decay.

### B. Directed-detection quantum trajectory unravelling

Following the proposal of Carmichael and Kim [28], we unravel the master equation into quantum trajectories based on direct photon counting. Thus, the density operator is decomposed as a sum over pure states:

$$\rho(t)=\sum_{\mathrm{REC}} P_{\mathrm{REC}}|\psi_c(t)\rangle\langle\psi_c(t)|, \tag{6}$$

where REC is the record denoting a particular sequence of photon detections (emissions), up to time $t$ and $P_{\mathrm{REC}}=\langle\overline{\psi}_c(t)|\overline{\psi}_c(t)\rangle$ is the probability for that record to occur. States $|\psi_c(t)\rangle$ and $|\overline{\psi}_c(t)\rangle$ are the normalized and unnormalized states, respectively, of the atoms conditioned on the occurrence of the sequence REC.

The time evolution of $|\overline{\psi}_c(t)\rangle$ is generated by a non-Hermitian Hamiltonian and punctuated by jumps generated by a set of jump operators at the times of photon emissions. For a general master equation in Lindblad form,

$$\dot{\rho}=-\frac{i}{\hbar}[\hat{H},\rho]+\sum_i (2\hat{O}_i\rho\hat{O}_i^\dagger-\hat{O}_i^\dagger\hat{O}_i\rho-\rho\hat{O}_i^\dagger\hat{O}_i), \tag{7}$$

the non-Hermitian Hamiltonian is

$$\hat{H}_B=\hat{H}-i\hbar\sum_i \hat{O}_i^\dagger\hat{O}_i, \tag{8}$$

and the jumps are generated by the set of operators $\hat{O}_i$ [23]. We use two approaches to cast the master equation in explicit Lindblad form, identifying two distinct sets of jump operators. The first, developed in detail by Carmichael and Kim [28], yields the directed-detection jump operators

$$\hat{S}(\theta,\phi)=\sqrt{\gamma D(\theta,\phi)d\Omega}\sum_{j=1}^{N} e^{-ik_0\hat{R}(\theta,\phi)\cdot\mathbf{r}_j}\hat{\sigma}_{j-}, \tag{9}$$

which apply when a photon is detected in the far field within the element of solid angle $d\Omega$ in direction $\hat{R}(\theta,\phi)$. Quantity

$$D(\theta,\phi)=\frac{3}{8\pi}\{1-[\hat{d}\cdot\hat{R}(\theta,\phi)]^2\} \tag{10}$$

is the dipole radiation pattern for emission from an isolated atom. For the $N$ atoms, an additional angular dependence enters through the propagation phase factors in Eq. (9). When diagonalized in terms of these jump operators, master equation (1) reads as

$$\dot{\rho}=-i\sum_{i\neq j=1}^{N}\Delta_{ij}[\hat{\sigma}_{i+}\hat{\sigma}_{j-},\rho]+\frac{1}{2}\int[2\hat{S}(\theta,\phi)\rho\hat{S}^\dagger(\theta,\phi) -\hat{S}^\dagger(\theta,\phi)\hat{S}(\theta,\phi)\rho-\rho\hat{S}^\dagger(\theta,\phi)\hat{S}(\theta,\phi)]. \tag{11}$$

Note that the jump operators for this unravelling have a clear physical interpretation in terms of the detection of outgoing photons in direction $(\theta,\phi)$.

### C. Source-mode quantum trajectory unravelling

Alternatively, we may identify jump operators by diagonalizing the matrix of the coefficients $(\gamma_{ij})$ [21,22]. This yields what Carmichael and Kim [28] call formal jump operators. As we will see, these jump operators draw their physical meaning from an expansion of the collective atomic polarization in source modes. They are not, therefore, so clearly identified with a particular photon detection event (however, see Sec. IV A).

Matrix $(\gamma_{ij})$ is a real symmetric matrix which can be diagonalized by an orthogonal transformation of the form

$$(\gamma_{ij})=\boldsymbol{B}^T\boldsymbol{\Lambda}\boldsymbol{B}, \tag{12}$$

where

$$\boldsymbol{\Lambda}\equiv\mathrm{diag}(\lambda_1,\ldots,\lambda_N) \tag{13}$$

is a diagonal matrix of the eigenvalues of $(\gamma_{ij})$ and the columns of $\boldsymbol{B}^T=(b_{ij})^T$,

$$\boldsymbol{b}_l\equiv\begin{pmatrix} b_{l1}\\ \vdots\\ b_{lN}\end{pmatrix}, \tag{14}$$

are the corresponding normalized eigenvectors. The master equation is written in this unravelling as

$$\dot{\rho}=-i\sum_{i\neq j=1}^{N}\Delta_{ij}[\hat{\sigma}_{i+}\hat{\sigma}_{j-},\rho] +\frac{1}{2}\sum_{l=1}^{N}(2\hat{J}_l\rho\hat{J}_l^\dagger-\hat{J}_l^\dagger\hat{J}_l\rho-\rho\hat{J}_l^\dagger\hat{J}_l), \tag{15}$$

where the source-mode jump operators are

$$\hat{J}_l=\sqrt{\lambda_l}\boldsymbol{b}_l^T\hat{\boldsymbol{\Sigma}},\quad \hat{J}_l^\dagger=\sqrt{\lambda_l}\hat{\boldsymbol{\Sigma}}^\dagger\boldsymbol{b}_l, \tag{16}$$

where we define

$$\hat{\boldsymbol{\Sigma}}\equiv\begin{pmatrix}\hat{\sigma}_{1-}\\ \vdots\\ \hat{\sigma}_{N-}\end{pmatrix},\quad \hat{\boldsymbol{\Sigma}}^\dagger\equiv(\hat{\sigma}_{1+},\ldots,\hat{\sigma}_{N+}). \tag{17}$$

Like the directed-detection jump operators, the source-mode jump operators are collective atomic operators.

### D. Angular distribution for the *k*th emitted photon

Our aim is to follow the evolution of the angular distribution for photon emission from the dipole radiation pattern, which holds for the first emitted photon, to a directed distribution of the sort suggested by earlier theories of super-

radiance. Our chosen path to this goal is a calculation of the angular distribution for the $k$th emitted photon; thus, we aim to calculate the probability for the $k$th photon to be emitted within the solid angle $d\Omega$ in direction $(\theta,\phi)$.

One possible expression for this probability is obtained using jump operator (9) for all $k$ emissions [30] and then integrating over the directions of the first to the $(k-1)$th emissions. This approach is not found to be very useful, though, because even for a few atoms the integration over emission directions is cumbersome to perform analytically and difficult to evaluate accurately in numerical simulations. We use an alternative expression, adopting source-mode jump operators for the first $k-1$ emissions and jump operator (9) for the $k$th emission only. We then sum over a finite number $N$ of alternate entries in the record, on each photon emission. From a straightforward elaboration of the sum in Eq. (6) and the explicit expression for the time evolution of $|\overline{\psi}_c(t)\rangle$, we write

$$P_k(\theta,\phi)d\Omega=\sum_{l_1=1}^{N}\cdots\sum_{l_{k-1}=1}^{N}\int_0^\infty dt_1\cdots\int_{t_{k-1}}^\infty dt_k\langle\overline{\psi}_{l_1,t_1;\ldots l_{k-1},t_{k-1};\theta,\phi,t_k}|\overline{\psi}_{l_1,t_1;\ldots l_{k-1},t_{k-1};\theta,\phi,t_k}\rangle, \tag{18}$$

where

$$|\overline{\psi}_{l_1,t_1;\ldots l_{k-1},t_{k-1};\theta,\phi,t_k}\rangle=\hat{S}(\theta,\phi)\hat{B}(t_k-t_{k-1})\hat{J}_{l_{k-1}}\hat{B}(t_{k-1}-t_{k-2})\cdots\hat{J}_{l_1}\hat{B}(t_1)|\{+\}\rangle, \tag{19}$$

with

$$\hat{B}(\tau)\equiv\exp(-i\hat{H}_B\tau/\hbar), \tag{20}$$

and $|\{+\}\rangle$ denotes the initial state with all $N$ atoms excited. The non-Hermitian Hamiltonian is given by

$$\hat{H}_B=\hbar\sum_{i\neq j=1}^{N}\Delta_{ij}\hat{\sigma}_{i+}\hat{\sigma}_{j-}-i\hbar\frac{1}{2}\sum_{l=1}^{N}\hat{J}_l^\dagger\hat{J}_l. \tag{21}$$

The sum over records in Eq. (18) covers all permutations of source modes and emission times for the first $k-1$ emissions.

We specialize, in what follows, to a line of atoms located at $\boldsymbol{r}_j=(j-1)(s\lambda_0)\hat{\boldsymbol{z}}$, $j=1,\ldots,N$, where $s$ is the atomic separation in units of the resonant wavelength. The atomic dipole moments are all aligned perpendicular to the axis of line $\hat{\boldsymbol{z}}$. In view of the cylindrical symmetry, the phase factors in Eq. (9) are functions of polar angle $\theta$ only; the $\phi$ dependence is all contained in the dipole radiation pattern (10). It is therefore convenient to integrate $P_k(\theta,\phi)$ over azimuthal angle, which is effected by replacing $S(\theta,\phi)$ with

$$\hat{S}(\theta)=\sqrt{\gamma D(\theta)\sin\theta d\theta}\sum_{j=1}^{N}e^{-i2\pi(j-1)s\cos\theta}\hat{\sigma}_{j-}, \tag{22}$$

where

$$D(\theta)=(3/4)(1-\sin^2\theta/2). \tag{23}$$

From Eq. (18), the angular distribution of the first photon emission is

$$P_1(\theta)\sin\theta d\theta=\int_0^\infty dt_1\langle\overline{\psi}_{\theta,t_1}|\overline{\psi}_{\theta,t_1}\rangle, \tag{24}$$

where

$$|\overline{\psi}_{\theta,t_1}\rangle=\hat{S}(\theta)\hat{B}(t_1)|\{+\}\rangle=e^{-(N\gamma/2)t_1}\hat{S}(\theta)|\{+\}\rangle. \tag{25}$$

We substitute for $\hat{S}(\theta)$ from Eq. (22) and note that the interference terms have zero expectation in the excited state irrespective of the number of atoms. Hence,

$$P_1(\theta)=D(\theta); \tag{26}$$

the first photon is always emitted according to the dipole radiation pattern. We are interested in the development of $P_k(\theta)$ for $k>1$.

## III. EMISSION FROM A FEW ATOMS IN A LINE

As a first step, we briefly review the case of two atoms treated by Lehmberg [18] and others [6,19]. Lehmberg solved the master equation in a standard way to calculate the average photon emission rate as a function of direction. He obtained the dipole radiation pattern, in seeming contradiction with the directional correlations noted by Dicke [1]; in Lehmberg's words [18]: ''These results, especially (20), seem to contradict the prediction of photon-correlation arguments[7] that the radiative coupling between $A_1$ and $A_2$ enhances emission in certain directions.'' In Sec. III A we reproduce Lehmberg's result; we show that the second photon, like the first, is emitted with the dipole radiation pattern. In Sec. III B we show, however, that the two-atom case is special and an additional angular dependence appears as soon as three atoms are considered. We derive the angular distribution for three atoms analytically, omitting dipole-dipole interactions. In Sec. III C we numerically verify the result, with dipole-dipole interactions included. We then extend our numerical investigation to consider the case $N=11$.

### A. Two atoms: Lehmberg observation

There is only the second photon emission to consider. From Eq. (18), the angular distribution of the second emitted photon is given, for $N$ atoms, by

$$P_2(\theta)\sin\theta d\theta = \sum_{l_1=1}^{N} \int_0^\infty dt_1 \int_{t_1}^\infty dt_2 \langle \overline{\psi}_{l_1,t_1;\theta,t_2} | \overline{\psi}_{l_1,t_1;\theta,t_2} \rangle, \tag{27}$$

where

$$|\overline{\psi}_{l_1,t_1;\theta,t_2}\rangle = \hat{S}(\theta)\hat{B}(t_2-t_1)\hat{J}_{l_1}\hat{B}(t_1)|\{+\}\rangle = e^{-\gamma t_1}\hat{S}(\theta)\hat{B}(t_2-t_1)\hat{J}_{l_1}|\{+\}\rangle, \tag{28}$$

and the sum in Eq. (27) is over the $N$ possible first-emission jumps. It is helpful to note that the state reached after the first jump,

$$|l_1\rangle \equiv \hat{J}_{l_1}|\{+\}\rangle = \sqrt{\lambda_{l_1}}\boldsymbol{b}_{l_1}^T\hat{\boldsymbol{\Sigma}}|\{+\}\rangle, \tag{29}$$

is an eigenstate of operator $\Sigma_{l=1}^N \hat{J}_l^\dagger \hat{J}_l$; we have (Appendix A)

$$\left(\sum_{l=1}^{N} \hat{J}_l^\dagger \hat{J}_l\right)|l_1\rangle = [(N-2)\gamma + \lambda_{l_1}]|l_1\rangle. \tag{30}$$

Then, specializing to a pair of atoms, we write

$$(\gamma_{ij}) = \begin{pmatrix} \gamma & \Gamma \\ \Gamma & \gamma \end{pmatrix}, \tag{31}$$

with eigenvalues and eigenvectors given by

$$\lambda_{1,2} = \gamma \pm \Gamma \tag{32}$$

and

$$\boldsymbol{b}_1 = \frac{1}{\sqrt{2}}\begin{pmatrix} 1 \\ 1 \end{pmatrix}, \quad \boldsymbol{b}_2 = \frac{1}{\sqrt{2}}\begin{pmatrix} 1 \\ -1 \end{pmatrix}, \tag{33}$$

respectively. The jump operators for a pair of atoms, Eq. (16), are then

$$\hat{J}_1 = \sqrt{\gamma+\Gamma}\frac{\hat{\sigma}_{1-}+\hat{\sigma}_{2-}}{\sqrt{2}}, \tag{34a}$$

$$\hat{J}_2 = \sqrt{\gamma-\Gamma}\frac{\hat{\sigma}_{1-}-\hat{\sigma}_{2-}}{\sqrt{2}}. \tag{34b}$$

In addition to satisfying Eq. (30), in the two-atom case only, state $|l_1\rangle$ is an eigenstate of the dipole-dipole interaction Hamiltonian (eigenvalue $\pm\hbar\Delta_{12}$) and hence, also of the non-Hermitian Hamiltonian $\hat{H}_B$ (eigenvalue $-i\hbar\lambda_{l_1}/2 \pm \hbar\Delta_{12}$). The computation of the between-jump evolution is therefore trivial, and from Eqs. (27) and (28), the angular distribution of the second emitted photon is

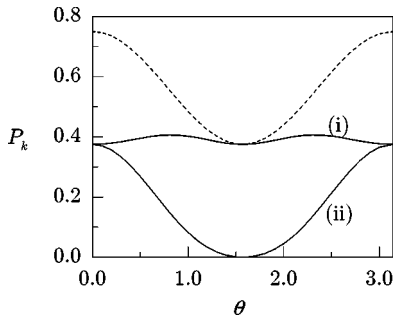


FIG. 1. Angular distribution of the second emitted photon following a first emission of type $J_1$ (i) and $J_2$ (ii); the two atoms are separated by $\lambda_0/4$. The dashed line shows the distribution (dipole pattern) summed over first emission type.

$$P_2(\theta) = D(\theta)\frac{1}{2}\sum_{l_1=1}^{2}\lambda_{l_1}^{-1}\langle l_1|(\hat{\sigma}_{1+}\hat{\sigma}_{1-}+\hat{\sigma}_{2+}\hat{\sigma}_{2-} + e^{-i\zeta}\hat{\sigma}_{1+}\hat{\sigma}_{2-}+e^{i\zeta}\hat{\sigma}_{2+}\hat{\sigma}_{1-})|l_1\rangle. \tag{35}$$

where $\zeta \equiv 2\pi s\cos\theta$.

The two terms in the sum cover the cases of a first emission of type $J_1$ and a first emission of type $J_2$. Their separate angular dependences are plotted in Fig. 1, where they are compared with the sum. The sum agrees with Lehmberg's result; it is again the dipole radiation pattern. Although the interference terms play a role in the individual trajectories, which allows for the correlation noted by Dicke [1], their contribution cancels in the sum over records.

### B. Three atoms: Analytical results

We now show that a directional dependence beyond that of the dipole pattern arises for three atoms in a line. Dipole-dipole interactions are omitted for simplicity.

In the case of three atoms, the record acquires three branches following the first emission. Considering the first line of Eq. (28), the evolution generated by $\hat{B}(t_1)$ is trivial, producing an overall exponential decay at the rate $3\gamma/2$. Furthermore, with the dipole-dipole interactions omitted, states (29) are eigenstates of $\hat{H}_B/i\hbar$ with eigenvalues [Eqs. (21) and (30)]

$$\lambda_1' = -\frac{1}{2}(\gamma+\lambda_1), \quad \lambda_{2,3}' = -\frac{1}{2}(\gamma+\lambda_{2,3}). \tag{36}$$

From Eq. (28), we therefore have

$$|\overline{\psi}_{l_1,t_1;\theta,t_2}\rangle = e^{-(3/2)\gamma t_1}e^{-\lambda_{l_1}'(t_2-t_1)}\hat{S}(\theta)|l_1\rangle. \tag{37}$$

Then, the time integrals in Eq. (27) are convolutions of exponentials and yield

$$P_2(\theta)\sin\theta d\theta = \sum_{l_1=1}^{3}\frac{\langle l_1|\hat{S}^\dagger(\theta)\hat{S}(\theta)|l_1\rangle}{3\gamma(\gamma+\lambda_{l_1})}. \tag{38}$$

For the explicit construction of the source-mode jump operators, we write

$$(\gamma_{ij})=\begin{pmatrix}\gamma & \Gamma & \delta\\ \Gamma & \gamma & \Gamma\\ \delta & \Gamma & \gamma\end{pmatrix}, \tag{39}$$

with eigenvalues

$$\lambda_1=\gamma-\delta, \quad \lambda_{2,3}=\gamma+\frac{\delta}{2}\pm\sqrt{\frac{\delta^2}{4}+2\Gamma^2}, \tag{40}$$

and corresponding eigenvectors

$$\boldsymbol{b}_1=\frac{1}{\sqrt{2}}\begin{pmatrix}1\\0\\-1\end{pmatrix}, \quad \boldsymbol{b}_2=\frac{\sqrt{2}}{\sqrt{\lambda_2-\lambda_3}}\begin{pmatrix}\frac{1}{2}\sqrt{\lambda_2-\gamma}\\ \Gamma/\sqrt{\lambda_2-\gamma}\\ \frac{1}{2}\sqrt{\lambda_2-\gamma}\end{pmatrix},$$

$$\boldsymbol{b}_3=\frac{\sqrt{2}}{\sqrt{\lambda_2-\lambda_3}}\begin{pmatrix}\frac{1}{2}\sqrt{\gamma-\lambda_3}\\ -\Gamma/\sqrt{\gamma-\lambda_3}\\ \frac{1}{2}\sqrt{\gamma-\lambda_3}\end{pmatrix}. \tag{41}$$

The jump operators are then given by

$$\hat{J}_1=\sqrt{\lambda_1}\frac{1}{\sqrt{2}}(\hat{\sigma}_{1-}-\hat{\sigma}_{3-}), \tag{42a}$$

$$\hat{J}_2=\sqrt{\lambda_2}\frac{\sqrt{2}}{\sqrt{\lambda_2-\lambda_3}}\left(\frac{1}{2}\sqrt{\lambda_2-\gamma}\hat{\sigma}_{1-}+\frac{\Gamma}{\sqrt{\lambda_2-\gamma}}\hat{\sigma}_{2-}+\frac{1}{2}\sqrt{\lambda_2-\gamma}\hat{\sigma}_{3-}\right), \tag{42b}$$

$$\hat{J}_3=\sqrt{\lambda_3}\frac{\sqrt{2}}{\sqrt{\lambda_2-\lambda_3}}\left(\frac{1}{2}\sqrt{\gamma-\lambda_3}\hat{\sigma}_{1-}-\frac{\Gamma}{\sqrt{\gamma-\lambda_3}}\hat{\sigma}_{2-}+\frac{1}{2}\sqrt{\gamma-\lambda_3}\hat{\sigma}_{3-}\right). \tag{42c}$$

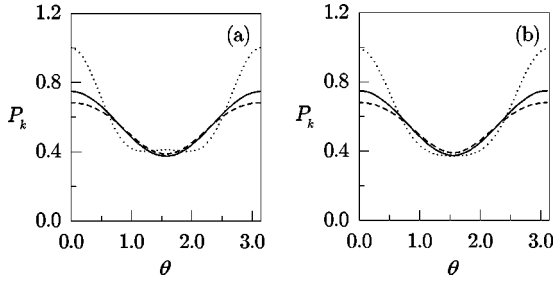


FIG. 2. Angular distributions of the first (solid line), second (dashed line), and third (dotted line) emitted photons for a line of three atoms separated by $\lambda_0/4$. Results excluding (a) and including (b) dipole-dipole interactions are presented.

Hence, using Eqs. (38) and (9), and substituting for $|l_1\rangle$ using Eqs. (29) and (42a)–(42c), the angular distribution of the second emitted photon is

$$P_2(\theta)=D(\theta)\frac{1}{3}\left\{\sum_{l_1=1}^{3}L_{l_1}+\frac{2\Gamma}{\lambda_2-\lambda_3}(L_2-L_3)\cos\zeta+\frac{1}{2}\left[-L_1+\frac{1}{\lambda_2-\lambda_3}((\lambda_2-\gamma)L_2+(\gamma-\lambda_3)L_3)\right]\cos 2\zeta\right\}, \tag{43}$$

with $\zeta\equiv 2\pi s\cos\theta$ and $L_l\equiv\lambda_l/(\gamma+\lambda_l)$.

The angular distribution of the third photon is obtained from a straightforward extension of these results. There is a further splitting of the record into three branches after the second emission. The distribution of the third emitted photon is therefore expressed as a sum of nine terms:

$$P_3(\theta)=\sum_{l_1,l_2=1}^{3}P_3^{l_1,l_2}(\theta), \tag{44}$$

where

$$P_3^{l_1,l_2}(\theta)\sin\theta d\theta=\int_0^\infty dt_1\int_{t_1}^\infty dt_2\int_{t_2}^\infty dt_3\, e^{-3\gamma t_1}e^{-(\gamma+\lambda_{l_1})(t_2-t_1)}|\langle\{-\}|\hat{S}(\theta)\hat{B}(t_3-t_2)\hat{J}_{l_2}|l_1\rangle|^2; \tag{45}$$

$|\{\}\rangle$ denotes the ground state with all atoms unexcited. The evaluation of $P_3^{l_1,l_2}(\theta)$ is sketched in Appendix B; the explicit results appear as Eqs. (B3a)–(B3i). In the three-atom case, the angular dependencies of the nine individual trajectories do not cancel in the sum and there is a distortion of the dipole radiation pattern for both the second and the third emitted photons. The result for the sum is shown in Fig. 2; the analytical expressions (43) and (44) are plotted in Fig. 2(a) and compared, in Fig. 2(b) with Monte Carlo simulations, including dipole-dipole interactions. The most prominent feature is the enhanced directionality of the third emitted photon, with an increased probability for emission near the axis of the line of atoms. The dipole-dipole interactions make only small alterations to the picture.

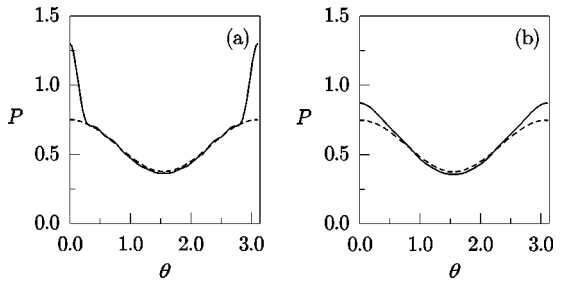


FIG. 3. Angular distribution of the total emission from a line of 11 atoms separated by $\lambda_0/4$. The dashed line shows the dipole pattern for comparison. Results excluding (a) and including (b) dipole-dipole interactions are presented.

### C. A few atoms: Numerical simulations

The expectation drawn from previous work on superradiance is that directed emission is well developed midway through a super-radiant pulse. It is therefore somewhat surprising that the third, not the second emitted photon, shows greater directionality in Fig. 2. Possibly, three atoms is too few, and the behavior is different for a larger number of atoms. We have therefore extended our calculations by performing Monte Carlo simulations for up to $N=11$ atoms. Simulations for larger numbers are not feasible due to our limited computational resources.

The results of Monte Carlo simulations for 11 atoms are displayed in Figs. 3–5. Each curve is an average over 20 000 trajectories, where the evolution of the conditional state along each trajectory is calculated from a sequence of jumps and between-jump evolutions, as in Eq. (19). The jumps are executed by the source-mode operators $\hat{J}_l$, $l=1,\ldots,11$, with $l$-type jumps occurring at the rate

$$\langle\psi_c(t)|\hat{J}_l^\dagger\hat{J}_l|\psi_c(t)\rangle=\frac{\langle\overline{\psi}_c(t)|\hat{J}_l^\dagger\hat{J}_l|\overline{\psi}_c(t)\rangle}{\langle\overline{\psi}_c(t)|\overline{\psi}_c(t)\rangle}. \tag{46}$$

The between-jump evolution is generated by $\hat{B}(\tau)$. After $k-1$ photon emissions, the un-normalized conditional state is

$$|\overline{\psi}_c(t)\rangle=\hat{B}(t-t_{k-1})\hat{J}_{l_{k-1}}\ldots\hat{J}_{l_1}\hat{B}(t_1)|\{+\}\rangle. \tag{47}$$

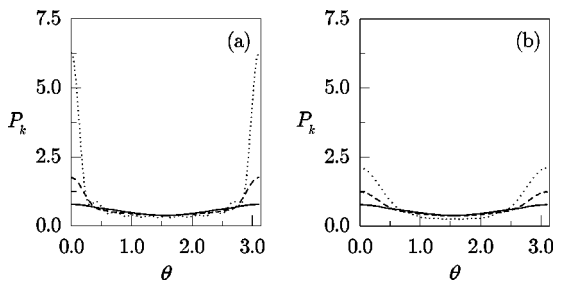


FIG. 4. Angular distributions of the ninth (solid line), tenth (dashed line), and eleventh (dotted line) emitted photons for a line of 11 atoms separated by $\lambda_0/4$. Results excluding (a) and including (b) dipole-dipole interactions are presented.

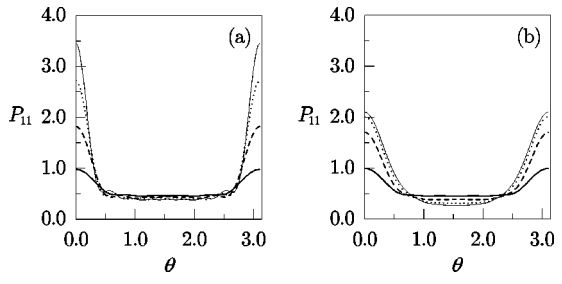


FIG. 5. Time-resolved angular distribution of the last emitted photon for a line of 11 atoms separated by $\lambda_0/4$; emission occurs before $\gamma t=1.0$ (bold solid line), 10.0 (dashed line), 100.0 (dotted line), and 1000.0 (light solid line). Results excluding (a) and including (b) dipole-dipole interactions are presented.

At the time of the $k$th photon emission (before executing jump $\hat{J}_{l_k}$), norm $\langle\overline{\psi}_c(t_k)|\hat{S}^\dagger(\theta)\hat{S}(\theta)|\overline{\psi}_c(t_k)\rangle$ is computed; the angular distribution of the $k$th emitted photon is the Monte Carlo average of this norm. From these averages, angular distributions are calculated for each of the 11 photons emitted in sequence. The angular distribution of the total emission is the sum of the 11 distributions.

In Fig. 3 we plot the angular distribution of the total emission. It deviates significantly from the dipole radiation pattern. As for the last photon emitted by three atoms, there is an increased probability for emission along the line of atoms, and the dipole-dipole interactions reduce, but do not eliminate the directionality.

The important question, though, is whether the directionality is associated with the superradiant enhancement of the spontaneous emission rate, which peaks halfway through the emission sequence. We address this question in Fig. 4, where we plot the angular distributions for the ninth, tenth, and eleventh emitted photons. Once again, the directionality is most pronounced for the last photon emission; even the ninth emission hardly shows any change from the dipole radiation pattern. It seems, then, that the directionality of Fig. 3 is not associated with the superradiant phase of the emission. Our results are consistent with those of Blank *et al.* [20] and disagree with Duncan and Stehle [19]. Further evidence against a superradiant interpretation is provided by Fig. 5. Here we correlate the angular distribution of the last emission, the 11th emission, with the waiting time after the tenth emission. The figure shows a correlation between increased directionality and longer waiting times, the exact opposite of a superradiant effect. Waiting times as long as 1000 spontaneous lifetimes contribute to the directional effect of Fig. 3. Similar features are observed whether or not the dipole-dipole interactions are included.

In summary, from our consideration of a few atoms, we can draw the following conclusions: (i) spontaneous emission from a line of $N\geqslant 3$ atoms shows departures from the dipole radiation pattern exhibited by emission from one and two atoms; (ii) the most prominent change is an increased tendency for photons late in the emission sequence (in particular the last photon) to be directed close to the axis of the line of atoms; (iii) late emissions close to the axis tend to be delayed—are subradiant rather than superradiant; and (iv)

dipole-dipole interactions change the results quantitatively, but do not alter the qualitative behavior. The overall conclusion is that 11 atoms in a line are too few to generate a directed superradiant pulse. Although superradiant enhancement of the emission rate is observed when the atoms are sufficiently close together, aside from small corrections, the superradiant phase of the emission is associated with a dipole radiation pattern. There is a directed subradiant phase, however, at the end of the photon emission sequence.

## IV. PROPERTIES OF THE SOURCE MODES

Some approximation is called for if we are to take our calculations significantly beyond $N=11$. To this end we turn, in this section, to a more detailed development of the formalism of Sec. II. For the remainder of the paper we neglect the dipole-dipole interactions.

### A. Relationship between directed and source-mode jump operators

Jump operator $\hat{S}(\theta)$ gains a physical interpretation through its association with the detection of a photon within a conical solid angle of thickness $d\theta$ and opening angle $\theta$. So far we have offered no physical interpretation for the source-mode jump operators. A straightforward interpretation would follow from an expansion of $\hat{J}_l$ in terms of $\hat{S}(\theta)$, but such an expansion does not exist; it is possible to expand $\hat{S}(\theta)$ in terms of $\hat{J}_l$, $l=1,\ldots,N$, but not the reverse. In this section we develop the relationship between $\hat{S}(\theta)$ and $\hat{J}_l$. Results derived here are used in Sec. V B to provide an interpretation for the source-mode jump operators.

The relationship between $\hat{S}(\theta)$ and $\hat{J}_l$ follows from Eqs. (16) and (22), both of which define collective operators as expansions over the single-atom operators $\hat{\sigma}_{j-}$, $j=1,\ldots,N$. Let use rewrite the two expansions. We define the vector of phase factors

$$\mathbf{\Pi}(\theta)\equiv\begin{pmatrix}\pi_1(\theta)\\ \vdots\\ \pi_N(\theta)\end{pmatrix}\equiv\begin{pmatrix}1\\ e^{-i2\pi s\cos\theta}\\ \vdots\\ e^{-i2\pi(N-1)s\cos\theta}\end{pmatrix}, \tag{48}$$

such that

$$\hat{S}(\theta)=\sqrt{\gamma D(\theta)d\theta}\,\mathbf{\Pi}^T(\theta)\hat{\mathbf{\Sigma}}, \tag{49}$$

and collect the source-mode annihilation and creation operators together in column and row vectors, defining

$$\hat{\boldsymbol{J}}\equiv\begin{pmatrix}\hat{J}_1\\ \vdots\\ \hat{J}_N\end{pmatrix}=\sqrt{\mathbf{\Lambda}}\boldsymbol{B}\hat{\mathbf{\Sigma}}, \tag{50a}$$

$$\hat{\boldsymbol{J}}^\dagger\equiv(\hat{J}_1^\dagger,\ldots,\hat{J}_N^\dagger)=\hat{\mathbf{\Sigma}}^\dagger\boldsymbol{B}^T\sqrt{\mathbf{\Lambda}}. \tag{50b}$$

Equation (49) is not invertible, but Eqs. (50a) and (50b) are. Thus, noting that $\boldsymbol{B}$ is an orthogonal matrix, we have

$$\hat{\mathbf{\Sigma}}=\boldsymbol{B}^T\sqrt{\mathbf{\Lambda}^{-1}}\hat{\boldsymbol{J}}, \tag{51a}$$

$$\hat{\mathbf{\Sigma}}^\dagger=\hat{\boldsymbol{J}}^\dagger\sqrt{\mathbf{\Lambda}^{-1}}\boldsymbol{B}, \tag{51b}$$

and then substituting for $\hat{\mathbf{\Sigma}}$ in Eq. (49) we arrive at the expansion

$$\hat{S}(\theta)=\sqrt{\gamma D(\theta)\sin\theta d\theta}\,\mathbf{\Xi}^T(\theta)\sqrt{\mathbf{\Lambda}^{-1}}\hat{\boldsymbol{J}}, \tag{52}$$

where

$$\mathbf{\Xi}(\theta)\equiv\begin{pmatrix}\xi_1(\theta)\\ \vdots\\ \xi_N(\theta)\end{pmatrix}=\boldsymbol{B}\mathbf{\Pi}(\theta). \tag{53}$$

From the orthogonality of $\boldsymbol{B}$ and Eq. (48), we note that

$$\mathbf{\Xi}^\dagger(\theta)\mathbf{\Xi}(\theta)=\mathbf{\Pi}^\dagger(\theta)\boldsymbol{B}^T\boldsymbol{B}\mathbf{\Pi}(\theta)=N. \tag{54}$$

Expansion (52) is a fundamental relationship. It allows us to associate an angular dependence with the source-mode jump operators in the following way. Note first that coefficients $\xi_l(\theta)$ in expansion (52) may be expressed as off-diagonal matrix elements of $\hat{S}(\theta)$ taken with respect to the vacuum state and the one-quantum collective excitations $|l\rangle\equiv(\hat{J}_l^\dagger/\sqrt{\lambda_l})|\{-\}\rangle$; we have

$$\frac{\langle\{-\}|\hat{S}(\theta)\hat{\boldsymbol{J}}^\dagger\sqrt{\mathbf{\Lambda}^{-1}}|\{-\}\rangle}{\sqrt{\gamma D(\theta)\sin\theta d\theta}}=\mathbf{\Xi}^T(\theta)\boldsymbol{B}\langle\{-\}|\hat{\mathbf{\Sigma}}\hat{\mathbf{\Sigma}}^\dagger|\{-\}\rangle\boldsymbol{B}^T$$
$$=\mathbf{\Xi}^T(\theta), \tag{55}$$

where we use $\langle\{-\}|\hat{\mathbf{\Sigma}}\hat{\mathbf{\Sigma}}^\dagger|\{-\}\rangle=\boldsymbol{I}_N$ and the orthogonality of $\boldsymbol{B}$. The expansion coefficients are then given by

$$\xi_l(\theta)=\frac{\langle\{-\}|\hat{S}(\theta)|l\rangle}{\sqrt{\gamma D(\theta)\sin\theta d\theta}}. \tag{56}$$

Using this expression, the angular distribution of emission from the one-quantum excitation $|l\rangle$ may be expressed in terms of $\xi_l(\theta)$. When the dipole-dipole interactions are neglected, $|l\rangle$ is an eigenstate of $\hat{H}_B$ (Appendix A), with

$$\hat{H}_B|l\rangle=-i\hbar\frac{1}{2}\hat{\boldsymbol{J}}^\dagger\hat{\boldsymbol{J}}|l\rangle=-i\hbar\frac{1}{2}\lambda_l|l\rangle. \tag{57}$$

It follows that $\hat{B}(t_1)|l\rangle=\exp(-\lambda_l t_1/2)|l\rangle$, and the angular distribution of emission with initial state $|l\rangle$ is

$$Q_l(\theta)\sin\theta d\theta = \int_0^\infty dt_1 \langle l|\hat{B}^\dagger(t_1)[\hat{S}^\dagger(\theta)\hat{S}(\theta)]\hat{B}(t_1)|l\rangle = (\gamma/\lambda_l)D(\theta)|\xi_l(\theta)|^2\sin\theta d\theta. \quad (58)$$

From Eq. (54), a weighted sum of these distributions returns the dipole radiation pattern:

$$\sum_{l=1}^N \lambda_l Q_l(\theta) = \gamma D(\theta)\sum_{l=1}^N |\xi_l(\theta)^2| = N\gamma D(\theta). \quad (59)$$

We see that $|\xi(\theta)|^2$ characterizes the difference between the radiation from the collective excitation $|l\rangle$ and the dipole radiation pattern. Moreover, an incoherent sum over excitations $|l\rangle$, $l=1,\ldots,N$, recovers the dipole radiation pattern. Examples of distribution $Q_l(\theta)$ are presented in Sec. V B.

More relevant to our interests are the properties of collective excitations near the fully excited state. The first photon is emitted according to the dipole distribution Eq. (26). Considered in terms of source modes, this result is an expression of sum rules (54) and (59); we have

$$\frac{\langle\{+\}|\hat{S}^\dagger(\theta)\hat{S}(\theta)|\{+\}\rangle}{\sin\theta d\theta} = \gamma D(\theta)\langle\{+\}|\hat{\mathbf{J}}^\dagger\sqrt{\mathbf{\Lambda}^{-1}}\mathbf{\Xi}^*(\theta)\mathbf{\Xi}^T(\theta)\sqrt{\mathbf{\Lambda}^{-1}}\hat{\mathbf{J}}|\{+\}\rangle = \gamma D(\theta)\sum_{l=1}^N |\xi_l(\theta)|^2 = \sum_{l=1}^N \lambda_l Q_l(\theta), \quad (60)$$

where we have used $\langle\{+\}|\hat{\mathbf{J}}^\dagger\hat{\mathbf{J}}|\{+\}\rangle = \mathbf{\Lambda}$. Assume that the first photon is emitted from source mode $l_1$. What, then, is the angular distribution of the second emitted photon? Let us define $|l_1\rangle = \hat{J}_{l_1}|\{+\}\rangle$, as in Eq. (29). The angular distribution of the second emitted photon, given the first emission is from source mode $l_1$, is then

$$\frac{P_2^{l_1}(\theta)\sin\theta d\theta}{\lambda_{l_1}/N\gamma} = \lambda_{l_1}^{-1}\int_0^\infty d\tau_2 \langle l_1|\hat{B}^\dagger(\tau_2)[\hat{S}^\dagger(\theta)\hat{S}(\theta)]\hat{B}(\tau_2)|l_1\rangle, \quad (61)$$

where $\tau_2 = t_2 - t_1$; $P_2^l(\theta)\sin\theta d\theta$ is the joint probability for the first photon to be emitted by mode $l_1$ *and* the second to be emitted in direction $\theta$, while $\lambda_l/N\gamma$ is the probability that the first photon is emitted by mode $l_1$. Equation (61) is similar to Eq. (58), but the integral is not as straightforward to evaluate because $|l_1\rangle$ is not an eigenstate of $\hat{H}_B$, even with the dipole-dipole interactions neglected. We can calculate the emission rate for small $\tau_2$, though. Denoting the conditional emission rate per unit solid angle by $R_2^{l_1}(\theta)$, this is given by

$$R_2^{l_1}(\theta) \equiv \frac{\langle\{+\}|\hat{J}_{l_1}^\dagger[\hat{S}^\dagger(\theta)\hat{S}(\theta)]\hat{J}_{l_1}|\{+\}\rangle}{\lambda_{l_1}\sin\theta d\theta} = \gamma D(\theta)\sum_{i,j=1}^N b_{l_1 i}b_{l_1 j}\sum_{n,m=1}^N \pi_n^*(\theta)\pi_m(\theta) \times\langle\{+\}|\hat{\sigma}_{i+}\hat{\sigma}_{n+}\hat{\sigma}_{m-}\hat{\sigma}_{j-}|\{+\}\rangle = \gamma D(\theta)\left[\left(\sum_{i,n=1}^N b_{l_1 i}^2|\pi_n(\theta)|^2 - \sum_{i=1}^N b_{l_1 i}^2|\pi_i(\theta)|^2\right) + \left(\sum_{i,n=1}^N b_{l_1 i}\pi_i(\theta)b_{l_1 n}\pi_n^*(\theta) - \sum_{i=1}^N b_{l_1 i}^2|\pi_i(\theta)|^2\right)\right]. \quad (62)$$

Since $|\pi_i(\theta)|^2 = 1$, each sum, except the third, is trivially constant. The third sum is evaluated, using Eq. (53), to be $|\xi_{l_1}(\theta)|^2$. We arrive at the result

$$R_2^{l_1}(\theta) = \gamma D(\theta)(N-2+|\xi_{l_1}(\theta)|^2). \quad (63)$$

Equation (63) is a generalization of the correlation, the stimulated emission enhancement factor, noted by Dicke [1]. Dicke observed that after the first emission in direction $\hat{\boldsymbol{k}}_1$, the rate for a second emission in the same direction is enhanced by a factor of two over that for spontaneous emission from independent atoms. The interpretation of Eq. (63) is not quite so straightforward, but a convincing demonstration of an enhancement of source mode $l_1$ can be given. Rate $R_2^{l_1}(\theta)$ may be divided into a factor $(N-1)\gamma D(\theta)$ which accounts for emission from $N-1$ independent atoms, plus an "enhancement" factor $\gamma D(\theta)(|\xi_{l_1}(\theta)|^2-1)$ whose angular distribution is that of the source mode from which the first photon was emitted. The enhancement may, in fact, be either positive or negative. Noting that the integral of either $D(\theta)$ or $Q_{l_1}(\theta)$ is unity, and using Eq. (58), we have

$$\int_0^\pi \sin\theta d\theta\, \gamma D(\theta)(|\xi_{l_1}(\theta)|^2-1) = \lambda_{l_1} - \gamma. \quad (64)$$

The eigenvalue spectrum is discussed in Sec. V A. For superradiant source modes ($\lambda_{l_1} > \gamma$), Eq. (64) indicates a positive enhancement; for subradiant modes ($\lambda_{l_1} < \gamma$) the enhancement is negative—an inhibition.

### B. Boson approximation for many atoms

The angular properties of the source modes described in the preceding section are helpful, but limited in what they tell us about the development of directional superradiant emission. We identified the directionality of certain collective excitations of the atoms, but nothing was said about the dynamical process, about the between-jump evolution and the sequence of states visited as the spontaneous emission proceeds. In this section we formulate an approximation which allows us to address these limitations.

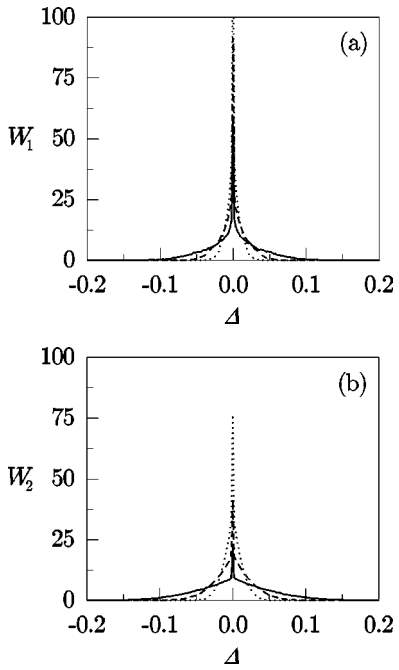


FIG. 6. Distribution of the commutator deviation Eq. (69) (a) and Eq. (70) (b) for $N=50$ (solid line), 100 (dashed line), and 200 (dotted line) atoms. The atoms are separated by $\lambda_0/4$.

The approximation is based on the observation that the source-mode operators act like boson operators near the fully excited state $|\{+\}\rangle$ or near the ground state $|\{-\}\rangle$, a result which follows from the fact that the sets of operators $\sqrt{\mathbf{\Lambda}^{-1}}\hat{\boldsymbol{J}}$ and $\hat{\boldsymbol{J}}^\dagger\sqrt{\mathbf{\Lambda}^{-1}}$ are formed from orthonormal eigenvectors of matrix $(\gamma_{ij})$. Consider the commutator

$$(\lambda_l\lambda_{l'})^{-1/2}[\hat{J}_l^\dagger,\hat{J}_{l'}]=\sum_{i=1}^{N} b_i^l b_i^{l'}\hat{\sigma}_{iz}, \tag{65}$$

where we use definition (16) and $[\hat{\sigma}_{i-},\hat{\sigma}_{j+}]=\delta_{ij}\hat{\sigma}_{iz}$. Acting with this commutator on states $|\{+\}\rangle$ and $|\{-\}\rangle$, we have

$$(\lambda_l\lambda_{l'})^{-1/2}[\hat{J}_l^\dagger,\hat{J}_{l'}]|\{\pm\}\rangle=\pm\boldsymbol{b}_l^T\boldsymbol{b}_{l'}|\{\pm\}\rangle=\pm\delta_{ll'}|\{\pm\}\rangle, \tag{66}$$

which shows that $\hat{J}_l^\dagger$ and $\hat{J}_{l'}$ act like the annihilation (creation) and creation (annihilation) operators of independent boson modes in state $|\{+\}\rangle$ ($|\{-\}\rangle$). More generally, if the commutator acts on a state that is $n\ll N$ excitations below $|\{+\}\rangle$, or $n\ll N$ above $|\{-\}\rangle$, the conclusion will hold to within a correction of order $n/N$. Armed with this observation, for large $N$ and excitations close to the fully excited state, we propose the following boson approximation:

$$\hat{J}_l\to\sqrt{\lambda_l}\hat{a}_l^\dagger \quad\text{with}\quad [\hat{a}_l,\hat{a}_{l'}^\dagger]=\delta_{l,l'}. \tag{67}$$

The boson creation operators $\hat{a}_l^\dagger$ create delocalized holes within a population of many excited atoms. Close to the ground state, we propose

$$\hat{J}_l^\dagger\to\sqrt{\lambda_l}\hat{b}_l^\dagger \quad\text{with}\quad [\hat{b}_l,\hat{b}_{l'}^\dagger]=\delta_{l,l'}; \tag{68}$$

the boson operators $\hat{b}_l^\dagger$ create delocalized excitations within a population of many unexcited atoms.

We have tested the scaling of approximation (67) with $n$ and $N$ for a line of atoms separated by $\lambda_0/4$. We numerically calculate the deviation of the commutator from $\delta_{ll'}$ for all $l$ and $l'$, and for all states $|l_1\rangle\equiv\hat{J}_{l_1}|\{+\}\rangle$ and $|l_1,l_2\rangle\equiv\hat{J}_{l_2}\hat{J}_{l_1}|\{+\}\rangle$ reached from $|\{+\}\rangle$ after one and two photon emissions. The distribution of computed deviations is presented in Fig. 6. Figure 6(a) plots probability density $W_1(\Delta)$, $\Delta\equiv\Delta^{(1)}_{l_1;l,l'}$ with

$$\Delta^{(1)}_{l_1;l,l'}\equiv\frac{\langle l_1|[\hat{J}_l^\dagger,\hat{J}_{l'}]|l_1\rangle}{\sqrt{\lambda_l\lambda_{l'}}\langle l_1|l_1\rangle}-\delta_{ll'}. \tag{69}$$

Figure 6(b) plots probability density $W_2(\Delta)$, $\Delta\equiv\Delta^{(2)}_{l_1,l_2;l,l'}$ with

$$\Delta^{(2)}_{l_1,l_2;l,l'}\equiv\frac{\langle l_1l_2|[\hat{J}_l^\dagger,\hat{J}_{l'}]|l_1l_2\rangle}{\sqrt{\lambda_l\lambda_{l'}}\langle l_1l_2|l_1l_2\rangle}-\delta_{ll'}. \tag{70}$$

As anticipated, the figures show the deviations decreasing and increasing with increasing $N$ and $n$, respectively.

The boson approximation brings an immense simplification. Without it, the source-mode operators only define a simplifying algebra in the Dicke, or single-mode limit. In the Dicke limit ($s\to0$) there is one superradiant eigenvalue $\lambda_N=N\gamma$ and the rest of the eigenvalues are zero (Sec. V A). $\hat{J}_N$ and $\hat{J}_N^\dagger$ are angular-momentum operators and the emission follows a straightforward sequence of jumps between the angular-momentum states $|J,M\rangle$, $J=N/2$, $M=N/2,\ldots,-N/2$: the conditional state following the $k$th jump is $|\psi_c(t_k^+)\rangle=|N/2,N/2-k\rangle$ and the between-jump evolution generates a trivial rescaling of state norm.

In the general multimode case, Eq. (65) offers no such simplification. There appears to be no alternative but to make the exact quantum trajectory evolution in the enormous Hilbert space of $N$ two-state atoms. The boson approximation (67) returns us to a situation where the operator algebra is simple and the bookkeeping of the conditional state evolution is straightforward. After the $k$th emission, the conditional state is

$$|\psi_{l_i,t_1;\ldots;l_k,t_k}\rangle=\prod_{l=1}^{N}|n_l\rangle\equiv|\{n_l\}_k\rangle, \tag{71}$$

with $\Sigma_{l=1}^N n_l=k$; $|\{n_l\}_k\rangle$ is a multimode Fock state and occupation numbers $n_l$, $l=1,\ldots,N$, count the holes created in the population of $N$ initially excited atoms. Then, the conditional emission rate per unit solid angle for the $(k+1)$th emitted photon is

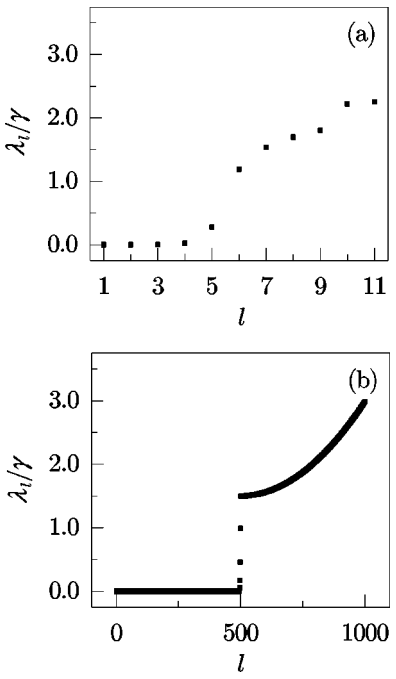


FIG. 7. Eigenvalues of the source modes for $N=11$ (a) and 1000 (b) atoms separated by $\lambda_0/4$.

$$R_{k+1}^{l_1,\ldots,l_k}(\theta)=\gamma D(\theta)\langle\{n_l\}_k|\hat{\boldsymbol{A}}^\dagger\sqrt{\boldsymbol{\Lambda}^{-1}}\boldsymbol{\Xi}^*(\theta)\times\boldsymbol{\Xi}^T(\theta)\sqrt{\boldsymbol{\Lambda}^{-1}}\hat{\boldsymbol{A}}|\{n_l\}_k\rangle=\gamma D(\theta)\sum_{l=1}^{N}|\xi_l(\theta)|^2(n_l+1), \tag{72}$$

where we define

$$\hat{\boldsymbol{A}}\equiv\begin{pmatrix}\sqrt{\lambda_1}\hat{a}_1^\dagger\\ \vdots\\ \sqrt{\lambda_N}\hat{a}_N^\dagger\end{pmatrix},\quad \hat{\boldsymbol{A}}^\dagger\equiv(\lambda_1\hat{a}_1,\ldots,\lambda_N\hat{a}_N). \tag{73}$$

Note that after a first emission from source mode $l_1$, the angular distribution for the second emission is given by

$$R_2^{l_1}(\theta)=\gamma D(\theta)(N+|\xi_{l_1}(\theta)|^2). \tag{74}$$

The rate differs from the exact result, Eq. (63), by something of order $1/N$; in place of Eq. (64), it yields the ''enhancement'' factor

$$\int_0^\pi \sin\theta d\theta\gamma D(\theta)(|\xi_{l_1}(\theta)|^2+1)=\lambda_{l_1}+\gamma. \tag{75}$$

Approximation (68) produces the exact result, Eq. (58), for the distribution of the one-quantum excitation. In the boson approximation, distributions $Q_l(\theta)$, $l=1,\ldots,N$, characterize the angular emission properties of the source modes quite generally. From Eqs. (58) and (72), we may write

$$R_{k+1}^{l_1,\ldots,l_k}(\theta)=\sum_{l=1}^{N}\lambda_l Q_l(\theta)(n_l+1), \tag{76}$$

which is a straightforward generalization of result (60) for emission from the fully excited state. The important additional factor is the bosonic stimulation by the hole occupation numbers $n_l$.

## V. EMISSION FROM MANY ATOMS IN A LINE

The bosonic stimulation will prove to be the fundamental driving mechanism of directional super-radiance. It translates into a differential amplification of the emission from different source modes at rates $\lambda_l$, $l=1,\ldots,N$. Eigenvalues $\lambda_l$ and angular distributions $Q_l(\theta)$ are therefore the basic ingredients around which the directed emission is formed. Before considering further Monte Carlo simulations, we briefly discuss some of the properties of these quantities. A more extensive discussion is given in a separate publication [29].

### A. Source-mode eigenvalues

In Fig. 7(a) we plot the eigenvalues for the line of 11 atoms that produced Figs. 3–5. They are compared with the eigenvalues for $N=1000$ atoms in Fig. 7(b). The eigenvalues are ordered according to their magnitude, from the smallest to the largest; there is no other significance to index $l$ of a particular eigenvalue.

In both examples, there is a clear distinction between eigenvalues that are smaller and larger than the independent-atom decay rate $\gamma$; the former are subradiant and the latter superradiant. The subradiant eigenvalues for 11 atoms are associated with long-delayed directional emission shown in Fig. 5. For $N=1000$ atoms, the majority of the subradiant eigenvalues are essentially zero. There are a few, however, that are nonzero and might be associated with similarly delayed directional emission.

In Fig. 7(b), the super-radiant eigenvalues appear to lie on a well-defined curve. There are, in fact, exactly $2Ns=500$ such eigenvalues, a number given (to the nearest integer) by twice the length of the line in units of the resonant wavelength. To a good approximation, these eigenvalues are determined by the dipole radiation distribution and spacing $s$ of the atoms, according to the formula (Sec. V B) [31]

$$\lambda_l/\gamma=s^{-1}D(\theta_l), \tag{77}$$

with

$$\cos\theta_l=\begin{cases}(q-1)/2Ns, & q=1,3,\ldots,\\ (q-2)/2Ns, & q=2,4,\ldots,\end{cases} \tag{78}$$

$l=N-2Ns+q$, $q=1,\ldots,2Ns$ (for $2Ns$ an integer). Adding atoms without changing the line length leaves the number of superradiant eigenvalues unchanged but increases their value by decreasing $s$; only the number of subradiant eigenvalues grows. Adding atoms to increase the line length increases the number of superradiant eigenvalues and gives a more closely spaced set of angles $\theta_l$.

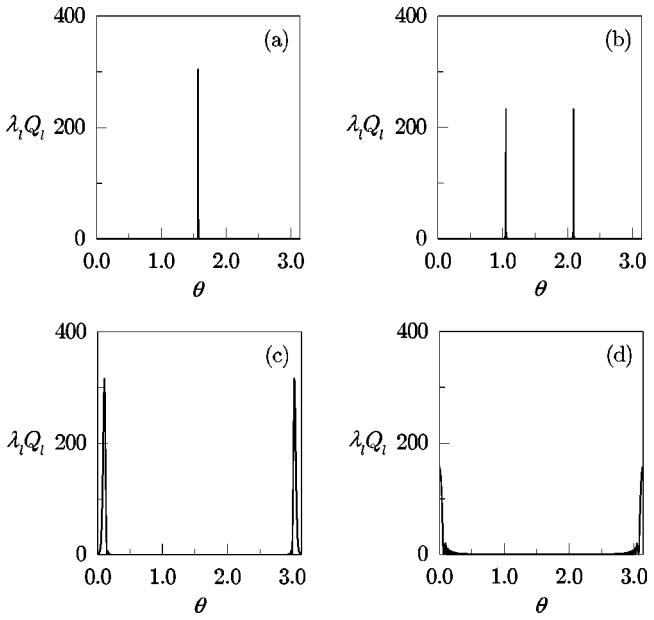


FIG. 8. Directionality of the source modes for $N=1000$ atoms separated by $\lambda_0/4$. The angular distribution of emission from the one-quantum excitation $\hat{J}_l^\dagger|\{-\}\rangle$ is plotted for modes $l=501$ (a), 750 (b), 1000 (c), and 500 (d).

We note from Eq. (59) (integrated over $\theta$) that the eigenvalues satisfy the sum rule

$$\sum_{l=1}^{N} \lambda_l = N\gamma. \tag{79}$$

In the Dicke, or single-mode limit, the length of the line shrinks to a point and matrix $(\gamma_{ij})$ has all entries equal to $\gamma$.

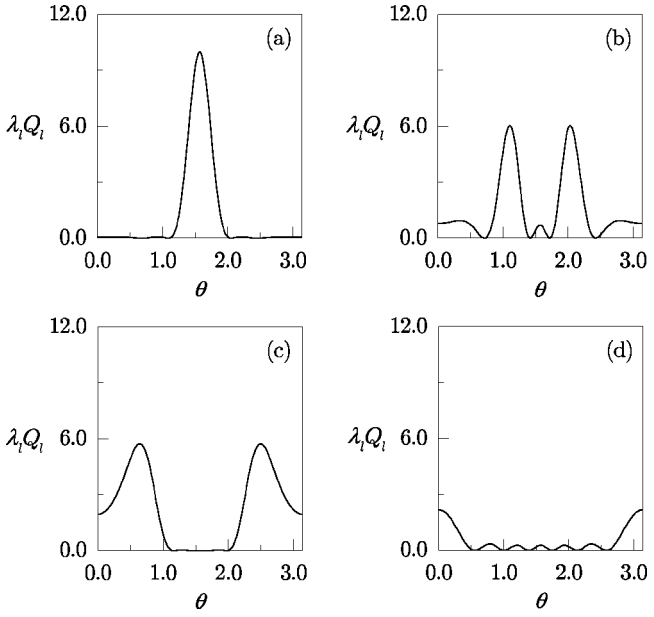


FIG. 9. Directionality of the source modes for $N=11$ atoms separated by $\lambda_0/4$. The angular distribution of emission from the one-quantum excitation $\hat{J}_l^\dagger|\{-\}\rangle$ is plotted for modes $l=7$ (a), 9 (b), 11 (c), and 5 (d).

There is then one superradiant eigenvalue $\lambda_N = N\gamma$ and $N-1$ subradiant eigenvalues all equal zero.

These properties of the eigenvalues are explained by considering the corresponding eigenfunctions and their associated emission patterns $Q_l(\theta)$.

### B. Source-mode eigenvectors and directionality

The source-mode emission patterns are determined from the eigenvectors using Eqs. (53) and (58). Representative examples are plotted in Figs. 8 and 9, where we plot $\lambda_l Q_l(\theta)$ for four values of $l$ to show the general pattern of behavior. The case of $N=1000$ atoms illustrates the behavior most clearly. There are $2Ns=500$ super-radiant eigenvalues with indices running from $l=501$ to $l=1000$. For $l=501$ (smallest superradiant eigenvalue), the source mode emits within a narrow disk perpendicular to the line of atoms [Fig. 8(a)]. Increasing the value of $l$, the emission is into a narrow conical solid angle opening at some $\theta_l < \pi/2$ relative to the line axis. Figure 8(b) shows the distribution for $l=750$. Angle $\theta_l$ decreases with increasing $l$. For $l=1000$ (largest superradiant eigenvalue), $\theta_l$ is small but nonzero, leaving a cone around the line axis that is excluded from the emission due to superradiant source modes [Fig. 8(c)].

According to Eq. (59), the sum over all $\lambda_l Q_l(\theta)$ yields the dipole radiation pattern. The excluded cone must therefore be filled by emission from the subradiant modes [and modes with eigenvalues in the transition region of Fig. 7(b)]. Indeed, we find that the emission patterns for the subradiant modes are all peaked along the axis; Fig. 8(d) shows the pattern for $l=500$. The result is as we might expect. Physically, subradiant decay rates arise from repeated emission and reabsorption (radiative trapping), which is more likely to occur for photons directed along the line of atoms.

The story for 11 atoms is qualitatively the same (Fig. 9) except that the distributions are significantly broader, as the line is a lot shorter.

Figure 9 makes it clear that the source-mode unravelling of Sec. II C has a different physical interpretation to the directed-emission unravelling of Sec. II B; the source modes do not emit in a single direction. For the parameters of Fig. 8, there is an approximate correspondence between the two unravellings, though, since the radiation from mode $l$ is confined to a narrow range of angles in the vicinity of some $\theta_l$ and $\pi-\theta_l$. In Fig. 9 also, the distributions are clearly peaked. This approximate directionality can be understood by considering a line that is many wavelengths long with a density of many atoms per wavelength, i.e., $N \gg 1$, $s \ll 1$, with $Ns \gg 1$. In this case, the super-radiant modes approximately make a Fourier decomposition of the atomic polarization on interval $0 \leqslant z \leqslant (N-1)s\lambda_0$ [29]. The eigenvectors are of the form

$$b_{lj} = \begin{cases} A_{lj}\sin[j(q-1)\pi/N + \phi_{lj}], & q=1,3,\ldots \\ A_{lj}\cos[j(q-2)\pi/N + \phi_{lj}], & q=2,4,\ldots, \end{cases} \tag{80}$$

where $A_{lj}$ and $\phi_{lj}$ vary slowly for changes in index, $\Delta j \sim 1/s$, corresponding to displacements along the line of the order of a wavelength. If we overlook the slowly varying

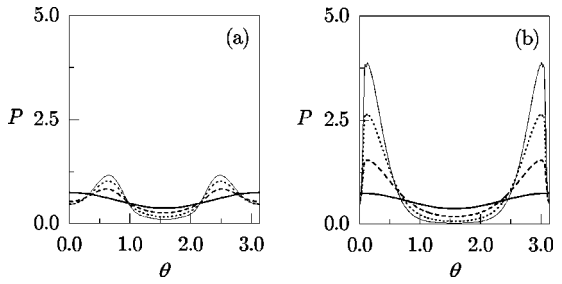


FIG. 10. Time-resolved angular distribution of the total emission, calculated within the boson approximation for a line of 11 atoms separated by $\lambda_0/4$ (a) and a line of 1000 atoms separated by $\lambda_0/40$ (b). Distributions are plotted for $\gamma t=0$ (bold solid line), 1.0 (dashed line), 2.0 (dotted line), and 3.0 (light solid line).

amplitude and phase, then radiation from mode $l$ interferes constructively in the far field at angles $\theta_l$ and $\pi-\theta_l$ for which the propagation phase difference, $2\pi s\cos\theta_l$, for adjacent atoms (atoms $j-1$ and $j$) is exactly canceled by the phase difference between their mode amplitudes ($b_{lj-1}$ and $b_{lj}$). This criterion yields Eq. (78) and an angle $\theta_l$ that closely tracks the positions of the peaks in Figs. 8(a)–8(c).

From Eq. (59), given the narrow distributions of Fig. 8, the corresponding eigenvalues are proportional to $D(\theta_l)$, and we can evaluate the proportionality constant from the eigenvalue sum rule (79) (setting all subradiant eigenvalues to zero). This calculation produces Eq. (77).

### C. Angular distribution of emission within the boson approximation

We are now in a position to consider the dynamical process that produces directed emission. Within the boson approximation (67), the dynamics is extremely simple. The conditional emission rate per unit solid angle, summed over source modes, is given by Eq. (76). It describes a stochastic evolution similar to the mode competition in a laser and gives rise to an average number of emissions (holes) per source mode, which grows exponentially in time; the hole occupation number for source mode $l$ amplifies at the rate $\lambda_l$. From Eq. (72), at time $t$ the mean directed-emission rate per unit solid angle is given by

$$\begin{aligned}\frac{\langle\hat{S}^\dagger(\theta)\hat{S}(\theta)\rangle(t)}{\sin\theta d\theta}&=\gamma D(\theta)\overline{\langle\{n_l\}_t|\hat{\mathbf{A}}^\dagger\sqrt{\mathbf{\Lambda}^{-1}}\mathbf{\Xi}^*(\theta)\mathbf{\Xi}^T(\theta)\sqrt{\mathbf{\Lambda}^{-1}}\hat{\mathbf{A}}|\{n_l\}_t\rangle}\\&=\gamma D(\theta)\sum_{l=1}^{N}|\xi_l(\theta)|^2e^{\lambda_l t},\end{aligned}\tag{81}$$

where $\{n_l\}_t$ is the set of hole occupation numbers at time $t$ and the overbar takes the stochastic average over $\{n_l\}_t$.

The intensity distribution (81) begins, for $t=0$, proportional to the dipole distribution $D(\theta)$ [Eq. (54)], and for long times approaches distribution $Q_N(\theta)$ of the source mode with largest eigenvalue. This evolution is illustrated in Fig. 10, for $N=11$ atoms with $s=0.25$ and $N=1000$ atoms with $s=0.025$; the curves are obtained as a Monte Carlo average over 20 000 trajectories. It is clear that as long as the amplification continues for sufficient time, the different amplification rates for different source modes eventually concentrates the emission into a cone near the line axis. There is a hole right on the axis, though, where the emission is dominated by the subradiant modes. We might associate the emission from individual source modes with the rays of Ernst and Stehle [6], but this process of mode competition is missing from their work.

In reality, the amplification may not continue for sufficient time; it terminates due to the depletion of the excitation energy. Energy depletion is an important feature neglected by the boson approximation. Without it, the approximation is clearly incapable of describing a superradiant *pulse*; moreover, if the $N$ initial quanta are emitted before sufficient amplification takes place, no significant directionality will develop at all.

We can estimate whether or not this is the case for the parameters of Fig. 10. We accept the boson approximation up until time $t_{N/2}$ when, on average, half the photons are emitted. We estimate $t_{N/2}$ by assuming all superradiant modes amplify at their mean rate, $\overline{\lambda}=\gamma/2s$, calculated from Eqs. (77) and (78). Thus, we write

$$2Ns\{\exp[(\gamma/2s)t_{N/2}]-1\}=N/2,\tag{82}$$

from which

$$\gamma t_{N/2}=2s\ln(1+1/4s).\tag{83}$$

The differential amplification of the axial relative to the side emission at $t_{N/2}$ is then given by

$$\exp\{s^{-1}\gamma[D(0)-D(\pi/2)]t_{N/2}\}=(1+1/4s)^{3/4}.\tag{84}$$

For $s=0.25$ (0.025), these results give $\gamma t_{N/2}=0.35$ (0.12) and a differential amplification of 1.7 (6.0). We conclude that the directionality shown in Fig. 10 is for times well beyond those for which the initial energy is depleted. Nevertheless, the estimated differential amplification suggests that a spacing $s=0.025$ will generate directionality within the duration of a superradiant pulse. On the other hand, the larger spacing $s=0.25$, seems to be marginal at best.

### D. An approximate treatment of atomic energy depletion

It is necessary to go beyond the simple boson approximation to make a reliable description of the development of directionality. We may do this by modifying the boson approximation to enforce energy depletion. We make two modifications. The first, and simpler, yields directional superradiant pulses, but misses the directed subradiant emission at long times [Figs. 4 and 5]. The second modification reproduces the subradiant emission also. It is difficult to assess the accuracy of the approximations since exact simulations are only possible when the number of atoms is small. Both approximations are exact, however, in the Dicke, or single-mode limit. The principle features in the development of

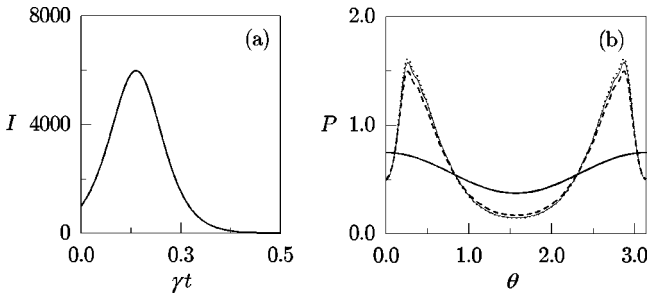


FIG. 11. Intensity (a) and time-resolved angular distribution of the total emission (b) calculated within the first modified boson approximation [Eq. (89)] for a line of 1000 atoms separated by $\lambda_0/40$. The distribution in (b) is calculated for $\gamma t=0$ (bold solid line), 0.15 (dashed line), 0.3 (dotted line), and 0.45 (light solid line).

directional superradiance appear to be accounted for, at least qualitatively, in the multimode case.

The modified boson approximations are introduced by altering the source-mode jump rates. In the boson approximation, the jump rates after the $k$th photon emission are given by the substitution

$$\langle \hat{J}_l^\dagger \hat{J}_l \rangle \rightarrow \lambda_l \langle \{n_{l'}\}_k | \hat{a}_l \hat{a}_l^\dagger | \{n_{l'}\}_k \rangle = \lambda_l (n_l + 1), \tag{85}$$

$l=1,\ldots,N$. The sum over these rates produces the net rate (76), integrated over angle $\theta$. The jumps in the boson approximation are executed by the hole creation operators $\hat{a}_l^\dagger$, $l=1,\ldots,N$. Consider now the single-mode limit, where there is one nonzero eigenvalue $\lambda_N$ with jump operator

$$\hat{J}_N = \sqrt{\lambda_N / N}\, \hat{J}_- , \tag{86}$$

where $\hat{J}_- = \Sigma_{j=1}^N \hat{\sigma}_{j-}$ is the Dicke collective operator. Adopting the Schwinger representation [32], the angular momentum algebra satisfied by $\hat{J}_-$, $\hat{J}_+$, and $\hat{J}_z$, is represented exactly by $\hat{J}_- = \hat{a}^\dagger \hat{b}$, $\hat{J}_+ = \hat{a}\hat{b}^\dagger$, $\hat{J}_z = \hat{b}^\dagger \hat{b} - \hat{a}^\dagger \hat{a}$, with $\hat{a}^\dagger \hat{a} + \hat{b}^\dagger \hat{b} = N$, where $a$ and $b$ are independent boson modes. Here $\hat{a}^\dagger$ creates a ground-state atom (equivalently an excited-state hole) and $\hat{b}$ annihilates an excited-state atom (equivalently a ground-state excitation). The conditional state after $k$ emissions is then represented as the two-boson-mode number state $|k\rangle_a |N-k\rangle_b$ and the exact jump rate is

$$\langle \hat{J}_N^\dagger \hat{J}_N \rangle = \lambda_N N^{-1} \langle (\hat{a}\hat{a}^\dagger)(\hat{b}^\dagger \hat{b}) \rangle = \lambda_N (1 - k/N)(n_N + 1). \tag{87}$$

The boson approximation (67) replaces $|N-k\rangle_b$ by $|N\rangle_b$; hence, it overlooks the depletion factor in the jump rate $(1 - k/N)$.

In order to approximately take the energy depletion in the multimode situation into account, we replace jump operator $\hat{a}_l^\dagger$ by $\hat{a}_l^\dagger \hat{b}$, where the boson mode $b$ counts the number of atoms remaining in the excited state: $\hat{b}^\dagger \hat{b} = N - \Sigma_{l=1}^N \hat{a}_l^\dagger \hat{a}_l$. The conditional state after $k$ emissions is then written as

$$|\psi_{l_1,t_1;\ldots;l_k,t_k}\rangle = |\{n_l\}_k\rangle_a |N-k\rangle_b , \tag{88}$$

and Eq. (85) is replaced by

$$\langle \hat{J}_l^\dagger \hat{J}_l \rangle \rightarrow \lambda_l (1 - k/N)(n_l + 1). \tag{89}$$

Note that any photon emission reduces the future emission rate of every source mode and therefore the modes are not independent in this approximation. The approximation is exact in the single-mode limit.

Figure 11 presents an example of a directional superradiant pulse obtained from the Monte Carlo simulation of 2000 trajectories using the first modified boson approximation. The parameters are the same as those of Fig. 10(b). The peak of the pulse occurs at $\gamma t \approx 0.16$, close to the predicted $\gamma t_{N/2} = 0.12$. There is also an evolution of the angular distribution as predicted, towards the cone emission of Fig. 10(b), but with the degree of directionality limited by the duration of the pulse. There is no directed subradiant emission in the tail of the pulse, however. This is not unexpected, since although energy depletion causes the source-mode amplification rates to decrease over time, the decrease applies uniformly to all eigenvalues. Thus, the amplification still continues throughout the entire pulse; the source modes with largest eigenvalues continue to dominate more and more over time. The second modified boson approximation corrects this deficiency.

The first modification is inadequate because according to Eq. (68), in the tail of the pulse we would expect to annihilate ground-state excitations with individual source-mode operators $\hat{b}_l$, while in fact we continue to create holes with operators $\hat{a}_l^\dagger$, annihilating excited-state atoms with the single operator $\hat{b}$. Stated in another way, Eqs. (67) and (68) suggest that the emission process should develop though *two* phases: (I) an initial amplification phase where stimulated hole creation dominates and (II) at the end of the pulse, a decay of the coherence produced through hole creation during the amplification phase. In an exact treatment, phase I would carry over into phase II in a gradual and continuous way. The second modified boson approximation implements it discontinuously, by using the jump operators $a_l^\dagger \hat{b}$, and rates (89), until half the photons are emitted, and then changing to jump operators $a_l^\dagger \hat{b}_l$ and adopting the conditional state ($k \geqslant N/2$)

$$|\psi_{l_1,t_1;\ldots;l_k,t_k}\rangle = |\{n_l\}_k\rangle_a |\{m_l\}_k\rangle_b , \tag{90}$$

with $\{m_l\}_k = 2\{n_l\}_{N/2} - \{n_l\}_k$; the jump rates for the second half of the pulse are

$$\langle \hat{J}_l^\dagger \hat{J}_l \rangle \rightarrow \lambda_l \frac{m_l (n_l + 1)}{2 m_l^{\max}}. \tag{91}$$

In this approximation, the source modes emit independently through the second half of the pulse. To achieve the independence, we have arbitrarily replaced state $|\{n_l\}_{N/2}\rangle_a |N/2\rangle_b$ reached after $N/2$ emissions by state $|\{n_l\}_{N/2}\rangle_a |\{n_l\}_{N/2}\rangle_b$, effectively equating number $n_l$ of excited-state holes created in mode $l$ during the growth of the pulse with the number of ground-state excitations to be annihilated during its decay. Of course, it is not possible to implement the independent source-mode emission starting

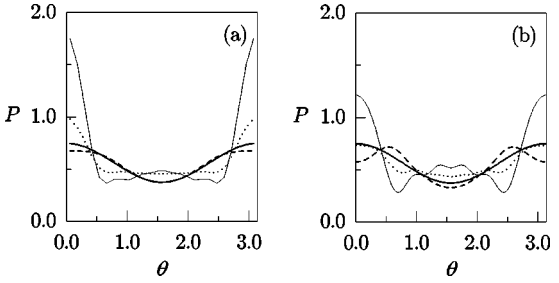


FIG. 12. Time-resolved angular distribution of the total emission from a line of 11 atoms separated by $\lambda_0/4$. The exact calculation (a) is compared with the second modified boson approximation [Eqs. (89) and (91)] (b). Distributions are calculated for $\gamma t=0$ (bold solid line), 1.0 (dashed line), 2.0 (dotted line), and 3.0 (light solid line).

out of the initial state, because there is no way to distribute the $N$ initial excitations between the different source modes; thus, we let mode competition during the first half of the pulse determine how the excitations are to be distributed amongst the different modes. The approximation is somewhat *ad hoc*, but is again exact in the single-mode limit. More importantly, it is also able to account for the subradiant emission displayed in Figs. 4 and 5.

We have implemented the second modified boson approximation as a Monte Carlo simulation and displayed examples of the results in Figs. 12–14. Figure 12 shows the result for 11 atoms and compares it with the exact quantum trajectory simulation. Although the quantitative agreement is not very good ($N$ is still small), the comparison lends credibility to the approximation. Note, in particular, that the directed subradiant emission is now reproduced in the tail of the pulse. From the approximation, we can identify a physical mechanism behind this late emission. It occurs because for any subradiant mode that emits spontaneously during the early stages of the decay, an excited-state hole is created (occupation number $n_l=1$) and preserved as a unique coherence in the medium. Even if no significant amplification of mode $l$ takes place as the superradiance develops, the established coherence remains to decay slowly at the end of the pulse.

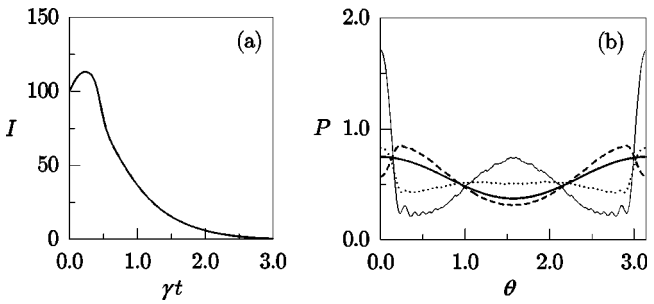


FIG. 13. Intensity (a) and time-resolved angular distribution of the total emission (b) calculated within the second modified boson approximation [Eqs. (89) and (91)] for a line of 100 atoms separated by $\lambda_0/4$. The distribution in (b) is calculated for $\gamma t=0$ (bold solid line), 1.0 (dashed line), 2.0 (dotted line), and 3.0 (light solid line).

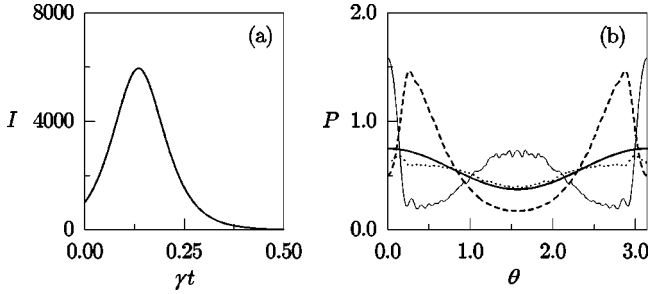


FIG. 14. Intensity (a) and time-resolved angular distribution of the total emission (b) calculated within the second modified boson approximation [Eqs. (89) and (91)] for a line of 1000 atoms separated by $\lambda_0/40$. The distribution in (b) is calculated for $\gamma t=0$ (bold solid line), 0.15 (dashed line), 0.3 (dotted line), and 0.45 (light solid line).

Figures 13 and 14 present results for larger numbers of atoms. Both show similar directed subradiant emission in the tail of the pulse. In Fig. 13, density $s=0.25$ is too small for the development of strong directional superradiance. Figure 14, however, uses the same parameters as Fig. 11. It shows the same superradiant cone emission around the peak of the pulse, but this is replaced by the directed subradiant emission pattern in the pulse tail. Note that the overall pulse shape is unaltered between Figs. 11(a) and 14(a). The second modified boson approximation changes only the angular distribution of emitted photons.

## VI. DISCUSSION

Spontaneous emission from a line of atoms provides a rudimentary generalization of the Dicke model of superradiance to an extended medium. It is sufficient as a model to show how directional superradiance develops during a single pulse, beginning with a dipole radiation pattern for the first emitted photon. The directionality shown in Figs. 11 and 14 is not particularly pronounced, though, and takes the form of cone emission rather than being peaked about the line axis. These details are peculiar to the one-dimensional array. By applying the analysis developed in this paper to three-dimensional arrays, we are able to obtain significantly more pronounced directionality, and with a maximum rather than minimum on-axis intensity [33]. We find, however, that even in the three-dimensional case, the initiation of superradiance is a multimode phenomenon, not fundamentally different from the process illustrated here; the common *a priori* assumption of emission into two ''endfire'' modes is an oversimplification [29]. This is in fact clear without making a detailed analysis, since the first photon is emitted according to the dipole radiation pattern, which is to be formed from a sum over the angular distributions of all significant superradiant modes [Eq. (59)]. If those modes are highly directional, many necessarily contribute to form the required dipole pattern out of the sum. Subsequently, directional superradiance develops from a competition between the many modes during the early stages of the emission; a subset, not one, of the superradiant modes eventually dominate the rest.

A number of interesting and important questions are not

answered in this paper. We have not considered the dependence of the emission pattern on the orientation of the atomic dipoles, for example. The eigenvalue spectrum of Fig. 7(b) depends on this orientation. There is some interesting physics buried here as well. Specifically, for one particular orientation, the spectrum of superradiant eigenvalues is flat. This leads to the prediction that on average, the emission pattern follows the dipole distribution throughout the entire pulse [29]; thus, the *mean* angular distribution is that of the single-mode, Dicke model; differences from the Dicke model appear at the level of the shot-to-shot fluctuations [33].

The question of fluctuations has not been addressed at all in this paper. Considering Fig. 14, for example: is the single-pulse emission biased *either* forward of $\theta=\pi/2$ *or* backward of $\theta=\pi/2$, or more symmetrically distributed? What, more generally, are the shot-to-shot fluctuations? The simulations used for this paper can answer some [33], but not all such questions. Specifically, they impose shot-by-shot symmetry about $\theta=\pi/2$ due to the symmetry of the source modes (Figs. 8 and 9) on which the unravelling of the master equation is based (Sec. II C). Certainly, the symmetry holds in the mean, but it will not hold for single pulses in practice. A simulation of the full pulse statistics realized in the laboratory requires using the angle-resolved output modes that would illuminate a detector.

Questions also remain about the approximations we have used. The exact quantum trajectory formalism of Sec. II does not lead to anything so straightforward as a simple sequence of quantum jumps, not even a multimode sequence of jumps. Dicke discussed the angular correlation of successive photons in terms of such a sequence [30], but assuming ''intermolecular distances large, compared with a radiation wavelength.'' If neither this condition nor the condition that all radiators lie within a cubic wavelength holds, the collective emission dynamics accounted for by Eqs. (18)–(21) is more complex, involving a nontrivial between-jump evolution that takes place within the enormous Hilbert space of $N$ entangled two-state systems. The modified boson approximations of Sec. V D return us to a simple multimode jump sequence; but they are somewhat *ad hoc*. Many questions remain about their accuracy and the details of the radiation process that lie hidden in the Hilbert space of $2^N$ dimensions. We know from a simpler two-mode model, for example, that significant errors can be introduced by ignoring the between-jump evolution [34,35]. The dipole-dipole interactions, neglected in Secs. IV and V, should also be included to reach a more accurate description.

Finally, considering the Hilbert space of $N$ entangled two-state systems raises questions of concern to the field of quantum information. What physics, for example, does the entanglement account for? How is the entanglement retained by the collective source modes different from the entanglement *between* source modes, which our approximations neglect? Recent proposals for entanglement generation in atomic ensembles [36,37] set aside the kinds of issues addressed in this paper, adopting, for example, the single-mode approximation [37]. The application of our approach to problems of this sort can assess the importance of mode competition and its contribution to decoherence rates. Such issues are likely to be particularly important for ensembles of mesoscopic size. Another avenue for its application is to proposals for quantum information processing within decoherence-free subspaces [38,39], or approximately decoherence-free subspaces, e.g., those spanned by excitations of the many subradiant modes.

## VII. CONCLUSIONS

Using a quantum trajectory unravelling of the Lehmberg-Agarwal master equation for collective spontaneous emission, we have calculated the angular distribution $P_k(\theta,\phi)$ of the $k$th photon emitted by a linear array of $N$ initially excited two-state atoms, $k=1,\ldots,N$. The unravelling of the master equation is made in terms of source-mode quantum jumps which we associate with directed emission from collective atomic modes. Closed form expressions for two and three atoms were obtained and show that three is the minimum number of atoms to show a difference from the dipole radiation pattern. Monte Carlo simulations were carried out for up to 11 atoms, both with and without the dipole-dipole interactions included. We found delayed, or subradiant emissions directed along the axis of the linear array, but no evidence of the emission of a directional superradiant pulse. Our results are consistent with the previous work of Lehmeberg [18] and Blank *et al.* [20], and disagree with the calculations of Duncan and Stehle [19].

Considering the commutation relations obeyed by the source-mode jump operators in the many-atom limit, we showed that a boson approximation may be made near the fully excited state; we introduced boson jump operators that create delocalized holes in the excited population of atoms. Within this approximation, and using the properties of the source-mode eigenvalues and eigenvectors, we demonstrated that directional superradiance develops from a differential amplification of the source modes driven by stimulated hole creation. In this way, the emission pattern is directed into forwards and backwards cones aligned with the axis of the atoms. On axis, a local minimum intensity develops, due to the many subradiant modes, for which there is negligible amplification. A boson approximation for weak excitation was also introduced; the jump operators, in this case, annihilate delocalized excitations.

To complete the overall picture, we considered depletion of the initial excited-state energy and derived the condition that directional superradiance occurs if $(1+1/4s)^{3/4}\gg 1$, where $s$ is the atomic spacing in units of the resonant wavelength; the line of atoms must also be extended over many wavelengths so that the rays emitted by individual source modes are narrow. We developed two modified boson approximations to take energy depletion into account. Monte Carlo simulations show marginal directionality for $N=100$ atoms and $s=0.25$, while strong directional superradiance was obtained for $N=1000$ atoms and $s=0.025$. The simulations predict that the directed subradiance observed for 11 atoms occurs also in the tail of a superradiant pulse.

## ACKNOWLEDGMENTS

This work was supported by the National Science Foundation under Grant No. PHY-0099576 and by an IREX grant

from the Australian Research Council. The authors gratefully acknowledge the helpful contributions of Dominic Berry to the development of the simulation algorithms.

## APPENDIX A: VERIFICATION OF EQS. (30) AND (57)

We demonstrate that state $|l_1\rangle \equiv \hat{J}_{l_1}|\{+\}\rangle$, reached after the first jump, is an eigenstate of operator $\Sigma_{l=1}^{N}\hat{J}_l^\dagger \hat{J}_l = \hat{\boldsymbol{J}}^\dagger \hat{\boldsymbol{J}}$ with eigenvalue $(N-2)\gamma + \lambda_{l_1}$. Using Eqs.(14), (16), and (17), we write

$$\begin{aligned}\left(\sum_{l=1}^{N}\hat{J}_l^\dagger \hat{J}_l\right)|l_1\rangle &= \sqrt{\lambda_{l_1}}\sum_{l=1}^{N}\lambda_l \sum_{i,j,m=1}^{N} b_{li}b_{lj}b_{l_1 m}\hat{\sigma}_{i+}\hat{\sigma}_{j-}\hat{\sigma}_{m-}|\{+\}\rangle \\ &= \sqrt{\lambda_{l_1}}\sum_{l=1}^{N}\lambda_l \sum_{j\neq m=1}^{N}(b_{lj}b_{lj}b_{l_1 m}\hat{\sigma}_{m-} \\ &\quad + b_{lm}b_{lj}b_{l_1 m}\hat{\sigma}_{j-})\{+\}\rangle. \end{aligned} \tag{A1}$$

Then, from Eqs. (12)–(14), we note that

$$\sum_{l=1}^{N}\lambda_l b_{lj}b_{lj} = \gamma_{jj} = \gamma. \tag{A2}$$

Thus, evaluating the sum over the first term on the right-hand side of Eq. (A1), we have

$$\sum_{l=1}^{N}\lambda_l \sum_{j\neq m=1}^{N} b_{lj}b_{lj}b_{l_1 m}\hat{\sigma}_{m-} = (N-1)\gamma \boldsymbol{b}_{l_1}^T \hat{\boldsymbol{\Sigma}}, \tag{A3}$$

and evaluating the sum over the second term, we have

$$\begin{aligned}&\sum_{l=1}^{N}\lambda_l \sum_{j\neq m=1}^{N} b_{lm}b_{lj}b_{l_1 m}\hat{\sigma}_{j-} \\ &= \sum_{l=1}^{N}\lambda_l \sum_{j,m=1}^{N} b_{lm}b_{lj}b_{l_1 m}\hat{\sigma}_{j-} - \sum_{l=1}^{N}\lambda_l \sum_{j=1}^{N} b_{lj}b_{lj}b_{l_1 j}\hat{\sigma}_{j-} \\ &= \sum_{l=1}^{N}\lambda_l \delta_{l,l_1}\sum_{j=1}^{N} b_{lj}\hat{\sigma}_{j-} - \gamma\sum_{j=1}^{N} b_{l_1 j}\hat{\sigma}_{j-} = (\lambda_{l_1}-\gamma)\boldsymbol{b}_{l_1}^T \hat{\boldsymbol{\Sigma}}, \end{aligned} \tag{A4}$$

where we use the orthonormality of the eigenvectors of $(\gamma_{ij})$ and Eq. (A2). Finally, from Eqs. (A1), (A3), and (A4), we obtain

$$\left(\sum_{l=1}^{N}\hat{J}_l^\dagger \hat{J}_l\right)|l_1\rangle = [(N-2)\gamma + \lambda_{l_1}]|l_1\rangle. \tag{A5}$$

We also show that state $\hat{J}_l^\dagger|\{-\}\rangle$ reached through a one-quantum excitation is an eigenstate of operator $\hat{\boldsymbol{J}}^\dagger \hat{\boldsymbol{J}}$ with eigenvalue $\lambda_l$. Using Eqs. (14), (16), and (17), we have

$$\begin{aligned}\hat{\boldsymbol{J}}^\dagger \hat{\boldsymbol{J}}|l\rangle &= \sum_{l'=1}^{N}\hat{J}_{l'}^\dagger \sum_{i,j=1}^{N}\sqrt{\lambda_{l'}\lambda_l}b_{l'i}b_{lj}\hat{\sigma}_{i-}\hat{\sigma}_{j+}|\{-\}\rangle \\ &= \sum_{l'=1}^{N}\hat{J}_{l'}^\dagger \sqrt{\lambda_{l'}\lambda_l}\sum_{j=1}^{N} b_{jl'}b_{jl}|\{-\}\rangle = \lambda_l|l\rangle, \end{aligned} \tag{A6}$$

where we again use the orthonormality of the eigenvectors of $(\gamma_{ij})$.

## APPENDIX B: EVALUATION OF EQ. (45)

We summarize the intermediate steps in the calculation of the angular distribution of the third photon emitted by a line of three atoms. In Appendix A we demonstrate that states $|l_1\rangle \equiv \hat{J}_{l_1}|\{+\}\rangle$, $l_1 = 1,2,3$, reached after the first photon emission, are the eigenstates of $\hat{H}_B$ in the subspace spanned by $|-++\rangle$, $|+-+\rangle$, and $|++-\rangle$ (omitting dipole-dipole interactions). Let $|1\rangle'$, $|2\rangle'$, and $|3\rangle'$ denote the eigenstates of $\hat{H}_B$ in the subspace spanned by $|+--\rangle$, $|-+-\rangle$, and $|--+\rangle$, respectively. Again, in Appendix A, we show that these are states $\hat{J}_l^\dagger|\{-\}\rangle$, $l = 1,2,3$, reached through a one-quantum excitation. It follows that the primed and the unprimed eigenstates are both represented by vectors $\boldsymbol{b}_1$, $\boldsymbol{b}_2$, and $\boldsymbol{b}_3$ [Eq. (41)]. Then, using the jump operators (42a)–(42c), we find that the states reached after the second photon emission may be expressed as

$$\hat{J}_1|1\rangle = -\frac{\sqrt{2}}{\sqrt{\lambda_2-\lambda_3}}\left(\frac{\Gamma}{\sqrt{\lambda_2-\gamma}}|2\rangle' - \frac{\Gamma}{\sqrt{\gamma-\lambda_3}}|3\rangle'\right), \tag{B1a}$$

$$\hat{J}_1|2\rangle = -\frac{\sqrt{2}}{\sqrt{\lambda_2-\lambda_3}}\frac{\Gamma}{\sqrt{\lambda_2-\gamma}}|1\rangle', \tag{B1b}$$

$$\hat{J}_1|3\rangle = -\frac{\sqrt{2}}{\sqrt{\lambda_2-\lambda_3}}\frac{\Gamma}{\sqrt{\gamma-\lambda_3}}|1\rangle', \tag{B1c}$$

and

$$\hat{J}_2|1\rangle = -\frac{\sqrt{2}}{\sqrt{\lambda_2-\lambda_3}}\frac{\Gamma}{\sqrt{\lambda_2-\gamma}}|1\rangle', \tag{B1d}$$

$$\hat{J}_2|2\rangle = \frac{\sqrt{2}\Gamma}{(\lambda_2-\lambda_3)^{3/2}}[3\sqrt{\lambda_2-\gamma}|2\rangle' + \frac{3\gamma-\lambda_2-2\lambda_3}{\sqrt{\gamma-\lambda_3}}|3\rangle', \tag{B1e}$$

$$\begin{aligned}\hat{J}_2|3\rangle = \frac{1}{(\lambda_2-\lambda_3)^{3/2}}&[(3\gamma-\lambda_2-2\lambda_3)\sqrt{\lambda_2-\gamma}|2\rangle' \\ &+ (3\gamma-2\lambda_2-\lambda_3)\sqrt{\gamma-\lambda_3}|3\rangle'], \end{aligned} \tag{B1f}$$

and

$$\hat{J}_3|1\rangle = \frac{\sqrt{2}}{\sqrt{\lambda_2-\lambda_3}}\frac{\Gamma}{\sqrt{\gamma-\lambda_3}}|1\rangle', \tag{B1g}$$

$$\hat{J}_3|2\rangle = \frac{1}{(\lambda_2-\lambda_3)^{3/2}}[(3\gamma-\lambda_2-2\lambda_3)\sqrt{\lambda_2-\gamma}|2\rangle' + (3\gamma-2\lambda_2-\lambda_3)\sqrt{\gamma-\lambda_3}|3\rangle'], \tag{B1h}$$

$$\hat{J}_3|3\rangle = \frac{\sqrt{2}\Gamma}{(\lambda_2-\lambda_3)^{3/2}}\left(\frac{3\gamma-2\lambda_2-\lambda_3}{\sqrt{\lambda_2-\gamma}}|2\rangle' - 3\sqrt{\gamma-\lambda_3}|3\rangle'\right). \tag{B1i}$$

Eigenvalues $\lambda_1, \lambda_2$, and $\lambda_3$ are given by Eq. (40). Substituting these results into Eq. (45), the form of $\hat{B}(t_3-t_2)\hat{J}_{l_2}|l_1\rangle = \exp[-i\hat{H}_B(t_3-t_2)/\hbar]\hat{J}_{l_2}|l_1\rangle$ shows all the required time integrals to be convolutions of exponentials [the primed eigenvectors of $\hat{H}_B$ have eigenvalues $-\lambda_l/2$ (Appendix A)]. Thus, evaluating the convolutions and making use of the matrix elements

$$|\langle\{-\}|\hat{S}(\theta)|1\rangle'|^2 = 2\gamma D(\theta)\sin\theta d\theta \sin^2\zeta, \tag{B2a}$$

$$|\langle\{-\}|\hat{S}(\theta)|2\rangle'|^2 = 2\gamma D(\theta)\sin\theta d\theta \frac{\lambda_2-\gamma}{\lambda_2-\lambda_3} \times\left(\cos\zeta + \frac{\Gamma}{\lambda_2-\gamma}\right)^2, \tag{B2b}$$

$$|\langle\{-\}|\hat{S}(\theta)|3\rangle'|^2 = 2\gamma D(\theta)\sin\theta d\theta \frac{\gamma-\lambda_3}{\lambda_2-\lambda_3} \times\left(\cos\zeta - \frac{\Gamma}{\gamma-\lambda_3}\right)^2, \tag{B2c}$$

with $\zeta \equiv 2\pi s\cos\theta$, we find that the angular distribution of the third emitted photon is given by the sum of

$$P_3^{11}(\theta) = D(\theta)\frac{1}{3}\frac{\lambda_1^2}{(\gamma+\lambda_1)}\frac{4\Gamma^2}{(\lambda_2-\lambda_3)^2}\left(\frac{\alpha_2^2}{\lambda_2}+\frac{\alpha_3^2}{\lambda_3}-\frac{4\alpha_2\alpha_3}{\lambda_2+\lambda_3}\right), \tag{B3a}$$

$$P_3^{12}(\theta) = D(\theta)\frac{1}{3}\frac{\lambda_2}{(\gamma+\lambda_1)}\frac{4\Gamma^2}{(\lambda_2-\lambda_3)(\lambda_2-\gamma)}\sin^2\zeta, \tag{B3b}$$

$$P_3^{13}(\theta) = D(\theta)\frac{1}{3}\frac{\lambda_3}{(\gamma+\lambda_1)}\frac{4\Gamma^2}{(\lambda_2-\lambda_3)(\gamma-\lambda_3)}\sin^2\zeta, \tag{B3c}$$

and

$$P_3^{21}(\theta) = D(\theta)\frac{1}{3}\frac{\lambda_2}{(\gamma+\lambda_2)}\frac{4\Gamma^2}{(\lambda_2-\lambda_3)(\lambda_2-\gamma)}\sin^2\zeta, \tag{B3d}$$

$$P_3^{22}(\theta) = D(\theta)\frac{1}{3}\frac{\lambda_2^2}{(\gamma+\lambda_2)}\frac{4\Gamma^2}{(\lambda_2-\lambda_3)^4}\left[\frac{9(\lambda_2-\gamma)^2\alpha_2^2}{\lambda_2} + \frac{(\lambda_1-\lambda_3)^2\alpha_3^2}{\lambda_3} + \frac{12(\lambda_2-\gamma)(\lambda_1-\lambda_3)\alpha_2\alpha_3}{\lambda_2+\lambda_3}\right], \tag{B3e}$$

$$P_3^{23}(\theta) = D(\theta)\frac{1}{3}\frac{\lambda_2\lambda_3}{(\gamma+\lambda_2)}\frac{4\Gamma^2}{(\lambda_2-\lambda_3)^4}\left[\frac{(\lambda_1-\lambda_3)^2(\lambda_2-\gamma)\alpha_2^2}{\lambda_2(\gamma-\lambda_3)} + \frac{(\lambda_1-\lambda_2)^2(\gamma-\lambda_3)\alpha_3^2}{\lambda_3(\lambda_2-\gamma)} + \frac{2(\lambda_1-\lambda_3)(\lambda_1-\lambda_2)\alpha_2\alpha_3}{\lambda_2+\lambda_3}\right], \tag{B3f}$$

and

$$P_3^{31}(\theta) = D(\theta)\frac{1}{3}\frac{\lambda_3}{(\gamma+\lambda_3)}\frac{4\Gamma^2}{(\lambda_2-\lambda_3)(\gamma-\lambda_3)}\sin^2\zeta, \tag{B3g}$$

$$P_3^{32}(\theta) = D(\theta)\frac{1}{3}\frac{\lambda_2\lambda_3}{(\gamma+\lambda_3)}\frac{4\Gamma^2}{(\lambda_2-\lambda_3)^4}\left[\frac{(\lambda_1-\lambda_3)^2(\lambda_2-\gamma)\alpha_2^2}{\lambda_2(\gamma-\lambda_3)} + \frac{(\lambda_1-\lambda_2)^2(\gamma-\lambda_3)\alpha_3^2}{\lambda_3(\lambda_2-\gamma)} + \frac{2(\lambda_1-\lambda_3)(\lambda_1-\lambda_2)\alpha_2\alpha_3}{\lambda_2+\lambda_3}\right], \tag{B3h}$$

$$P_3^{33}(\theta) = D(\theta)\frac{1}{3}\frac{\lambda_3^2}{(\gamma+\lambda_3)}\frac{4\Gamma^2}{(\lambda_2-\lambda_3)^4}\left[\frac{9(\gamma-\lambda_3)^2\alpha_3^2}{\lambda_3} + \frac{(\lambda_1-\lambda_2)^2\alpha_2^2}{\lambda_2} - \frac{12(\gamma-\lambda_3)(\lambda_1-\lambda_2)\alpha_2\alpha_3}{\lambda_2+\lambda_3}\right], \tag{B3i}$$

where $\alpha_n \equiv \cos\zeta + \Gamma/(\lambda_n-\gamma)$.


[1] R.H. Dicke, Phys. Rev. **93**, 99 (1954).
[2] M. Gross and S. Haroche, Phys. Rep. **93**, 301 (1982).
[3] L.I. Men'shikov, Phys. Usp. **42**, 107 (1999).
[4] B. Schumacher, Phys. Rev. A **51**, 2738 (1995).
[5] N.E. Rehler and J.H. Eberly, Phys. Rev. A **3**, 1735 (1971).
[6] V. Ernst and P. Stehle, Phys. Rev. **176**, 1456 (1968).
[7] R. Bonifacio and G. Preparata, Phys. Rev. A **2**, 336 (1970).
[8] R. Bonifacio, P. Schwendimann, and F. Haake, Phys. Rev. A **4**, 302 (1971).
[9] R. Bonifacio and L.A. Lugiato, Phys. Rev. A **11**, 1507 (1975).
[10] R. Bonifacio and L.A. Lugiato, Phys. Rev. A **12**, 587 (1975).
[11] R. Bonifacio, P. Schwendimann, and F. Haake, Phys. Rev. A **4**, 854 (1971).
[12] V. Degiorgio and F. Ghielmetti, Phys. Rev. A **4**, 2415 (1971).
[13] F. Haake and R. Glauber, Phys. Rev. A **5**, 1457 (1972).
[14] L. Narducci, C.A. Coulter, and C.M. Bowden, Phys. Rev. A **9**,

829 (1974).
[15] L. Narducci, C.A. Coulter, and C.M. Bowden, Phys. Rev. A **9**, 999 (1974).
[16] R. Glauber and F. Haake, Phys. Rev. A **13**, 357 (1976).
[17] R. Glauber and F. Haake, Phys. Lett. **68A**, 29 (1978).
[18] R.H. Lehmberg, Phys. Rev. A **2**, 889 (1970).
[19] A. Duncan and P. Stehle, Phys. Rev. A **35**, 4181 (1987).
[20] H. Blank, M. Blank, K. Blum, and A. Faridani, Phys. Lett. **105A**, 39 (1984).
[21] E. Ressayre and A. Tallet, Phys. Rev. Lett. **37**, 424 (1976).
[22] E. Ressayre and A. Tallet, Phys. Rev. A **15**, 2410 (1977).
[23] H. J. Carmichael, *An Open Systems Approach to Quantum Optics*, Lecture Notes in Physics, New Series m: Monographs Vol. m18 (Springer, Berlin, 1993).
[24] A.A. Belavkin, B.Y. Zeldovich, A.M. Perelomov, and V.S. Popov, Zh. Eksp. Teor. Fiz. **56**, 264 (1969).
[25] R.H. Lehmberg, Phys. Rev. A **2**, 883 (1970).
[26] G.S. Agarwal, Phys. Rev. A **2**, 2038 (1970).
[27] G. S. Agarwal, *Quantum Statistical Theories of Spontaneous Emission and their Relation to Other Approaches*, Springer Tracts in Modern Physics Vol. 70 (Springer, Berlin, 1974).
[28] H.J. Carmichael and K. Kim, Opt. Commun. **179**, 417 (2000).
[29] L. Horvath, B. C. Sanders, and H. J. Carmichael (unpublished).
[30] Dicke's discussion of the angular correlation of successive photons beginning on page 108 of Ref. [1] is formulated in the language of quantum trajectories. He considers the detection of each emitted photon in the far field, and constructs the state after the emission of the first $s-1$ photons [Eq. (84)] conditioned on the sequence of directions, $\boldsymbol{k}_1, \ldots, \boldsymbol{k}_{s-1}$, of those emissions. The construction specifically corresponds to the density operator unravelling of Carmichael and Kim [28].
[31] Ressayre and Tallet [21,22] also calculate these eigenvalues, but make an approximation which results in the spectrum being entirely flat [29].
[32] J. J. Sakurai, *Modern Quantum Mechanics* (Addison-Wesley, Reading, MA, 1994), pp. 217–221.
[33] J. P. Clemens and H. J. Carmichael (unpublished).
[34] J.P. Clemens and H.J. Carmichael, Phys. Rev. A **65**, 023815 (2002).
[35] H. Nha and H.J. Carmichael, Phys. Rev. A **66**, 053806 (2002).
[36] M.D. Lukin and P.R. Hemmer, Phys. Rev. Lett. **84**, 2818 (2000).
[37] L.-M. Duan, J.I. Cirac, P. Zoller, and E.S. Polzik, Phys. Rev. Lett. **85**, 5643 (2000).
[38] G.M. Palma, K.-A. Suaominen, and A.K. Ekert, Proc. R. Soc. London, Ser. A **452**, 567 (1996).
[39] D.A. Lidar, I.L. Chuang, and K.B. Whaley, Phys. Rev. Lett. **81**, 2594 (1998).